Second-harmonic generation in magnetic colloids by orientation of the nanoparticles

J. Lenglet, A. Bourdon, J.-C. Bacri,* and R. Perzynski
Laboratoire d'Acoustique et Optique de la Matière Condensée,† Université Pierre et Marie Curie, Tour 13, boîte 78, 4 Place Jussieu, 75252 Paris Cedex 05, France

G. Demouchy
Pôle Scientifique, Université de Cergy Pontoise, 49 Avenue des Genottes, Boîte Postale 8428, 95806 Cergy Pontoise, France
(Received 2 August 1995; revised manuscript received 23 January 1996)

We show that an optical second harmonic (SH) is generated in a magnetic colloid if a static magnetic field which breaks the fluid isotropy is applied. We propose a statistical model in which all the magnetic nanoparticles are supposed to be identical with a nonzero complex second-order polarizability tensor bound to their magnetic moment. These grains align under a static magnetic field according to Boltzmann's statistics. The nonlinear second-order macroscopic electric susceptibility tensor, ruled by a Langevin-like model, is found to be zero without any applied magnetic field and to be an increasing function of its strength. The nonlinear susceptibility tensor of the colloidal solution exhibits an axial C_∞ (and not $C_{\infty v}$) symmetry around the magnetic field. The measurements of the generated SH intensity as a function of the applied field strength, in all the independent input and output electric polarization directions, are in perfect agreement with our model and confirm the expected C_∞ symmetry. Under oblique incidence and without any applied magnetic field, the surface SH is generated by particles adsorbed on the glass cell walls and orientated normally to the interfaces. The complex values of the nonzero elements of the second-order polarizability tensor (leading to the observed SH wave ellipticity) are determined with a high precision, as well as that of the particle magnetic moment. The magnetic size found for the nanoparticle is in accordance with those given by other methods and could imply quantum confinement effects. A correlation between the ferrite particle atomic structure and the magnetic moment is found to be responsible of the noncentrosymmetry and of the chirality of the colloid under applied magnetic field. [S0163-1829(96)03022-6]

INTRODUCTION

Optical second harmonic generation (SHG) is a technique frequently used in the optical investigation of materials[1] and as a tool for studying interfaces.[2,3] In the electric dipolar approximation, SHG is allowed neither in isotropic media nor in centrosymmetrical media. Since 1962, several SHG experiments have been performed in isotropic media (solids, fluids) or in noncentrosymmetrical molecules of liquid crystals poled by a surface[2,3] or by a static electric field.[4–8] The loss of their symmetry makes second-order phenomena possible. Kielich has proposed a model in which two independent mechanisms account for SHG in solutions of microsystems under an applied static electric field. In the first one, each microsystem bears a permanent electric dipolar moment and exhibits a nonlinear polarizability; then SHG arises from a statistical orientation. In the second one, the applied field induces a deformation in centrosymmetrical microsystems which in turn gives an induced nonlinear polarizability.[9] SHG has also been observed in solid-state magnetic systems in which isotropy is broken, either by applying a static magnetic field[10,11] or by the antiferromagnetic properties of the materials.[12]

We report an experiment and a theoretical study of second harmonic generation in a magnetic fluid[13] (MF) in which the isotropy is broken by applying a static external magnetic field. The magnetic fluids, which exhibit many attractive properties,[14] have already been studied by optical methods.[15] The magnetic fluid (or ferrofluid) we use is a colloidal suspension of magnetic particles in water; their mean diameter is about 10 nm. They are synthesized by a coprecipitation technique[16] and made of cobalt ferrite. Each particle is a magnetic monodomain. Without any external applied magnetic field, the permanent magnetic moments are randomly oriented and the colloidal suspension is optically isotropic. Under a magnetic field, the magnetic moments of the individual grains tend to align along it. In our ferrofluid, each magnetic moment is frozen in the grain crystalline lattice so that a rotation of the magnetic moment induces the same rotation of the grain.[17] The contributions in the SHG phenomenon of atomic or electronic deformations inside the particles or in their vicinity induced by the magnetic field are much smaller than those due to global grain rotations and then neglected here. We have assumed that the microscopic origin of SHG has to be investigated in the particles, i.e., that the macroscopic second-order polarization is simply the sum of the electric nonlinear dipolar moments of the noncentrosymmetrical independent particles. This is reinforced by the fact that the SH intensity is, for low concentrations, experimentally proportional to the square of the particle volume fraction, as it will be developed in a forthcoming paper. In order to connect the microscopic particle behavior to the macroscopic behavior of the whole fluid, we develop a statistical model derived from Kielich's work.[9] In our model, as already proved for birefringence,[18] the magnetic and the second-order electric properties of the particles are at first glimpse decoupled. They are only both bound to the crystal lattice of the grain. For simplicity (and it will be further

justified), we suppose that all the particles are identical; no strong change in the SH response is expected because of this assumption. At this stage of the model, we make no symmetry restriction at all, about their second-order polarizability tensor: contrarily to Kielich's model, we introduce the possibility for the particles to exhibit ''triclinic'' properties and not only to have a symmetry of rotation around their magnetic moment; it compels us to consider a new degree of freedom in the particle orientation.

The transmitted SH intensity is measured as a function of the magnetic field strength in various geometries so as to determine all the nonzero elements of the nonlinear electric susceptibility tensor of the magnetic fluid. The very good consistency between the experiments and the statistical model predictions allows us to evaluate some of the nonzero elements of the second-order polarizability tensor of an individual particle even with their complex values. Angular SHG experiments are also presented which increase the reliability of the model and provide by complementarity with the former main experiments, a more precise value of the second-order polarizability tensor of the particles. An unexpected surface effect, but quite consistent with the bulk statistical model, is also observed. All the measurements are difficult for three reasons: without phase matching, the phenomenon is weak (conversion efficiency about 10^{-13}); the magnetic fluid absorbs the fundamental optical beam (absorption coefficient of about 51 cm^{-1} for the sample used) and even more the generated second harmonic one (about 2800 cm^{-1}); the damage threshold of the material is low (about 60 MW/cm^2) compared to that of usual crystals used as frequency doublers,[19] and depends on its particle volume fraction through absorption phenomena.

In view of the numerical results obtained for the nonlinear polarizability of the colloidal particles, we are able to discuss the origin of their SHG activity. Our initial choice of allowing in the model, ''triclinic'' properties to the particles is justified by the fact that some critical elements present nonzero values. The cubic symmetry of the spinel ferrite material is lost in the actual nanoparticles because of their shape, their finite size, their boundary layer structure and because they are clothed by solvent molecules. It is evident from the beginning that the particles must be noncentrosymmetrical so as to exhibit a nonzero nonlinear second-order polarization but a precise study of the polarizability tensor elements shows that the particles are chiral too. These two particle properties, inconsistent with those of the bulk ferrite material, will be discussed in the fifth paragraph about the origin of the particle SHG activity and in the conclusion together with their possibly enhanced nonlinear properties (quantum confinement).

I. PARTICLE ORIENTATION UNDER MAGNETIC FIELD: THEORETICAL SH MODEL

Our first step is to show theoretically how the isotropy of a colloidal magnetic fluid can be broken by a static magnetic applied field, to generate second harmonic. The complex amplitude components of the second-order polarization vector, induced in the medium by the complex amplitudes E_j^{ω} and E_k^{ω} of the components $E_j(t)$ and $E_k(t)$ of the electric field oscillating at the frequency ω, can be written as[20,21]

$$P_i^{2\omega} = d_{ijk} E_j^{\omega} E_k^{\omega},$$

where $E_j(t) = \mathrm{Re}[E_j^{\omega} e^{i\omega t}]$, $E_j^{-\omega} = (E_j^{\omega})^*$, and $P_i^{2\omega}(t) = \mathrm{Re}[P_i^{2\omega} e^{i2\omega t}]$. The complex third-rank tensor d_{ijk} is the second-order electric susceptibility. As $d_{ijk} = d_{ikj}$, $P_i^{2\omega}$ can be expressed with d_{im}, a contracted tensor written as a (3*6) matrix:[20]

$$P_i^{2\omega} = d_{im} (E^{\omega} E^{\omega})_m, \tag{1}$$

with the following conventions: $i = 1,2,3$ for x,y,z; $(EE)_m = E_m^2$ for $m = 1,2,3$; $(EE)_4 = 2E_y E_z$; $(EE)_5 = 2E_x E_z$; $(EE)_6 = 2E_x E_y$. In the electric dipole approximation, the tensor d_{ijk} of a medium exhibiting an inversion symmetry or isotropy is equal to zero and we must consider higher-order approximations (electric quadrupole, magnetic dipole approximations) to get nonzero components. These processes should be taken into account but we shall see they can be neglected in this study. An applied static magnetic field breaks the symmetry of the fluid by introducing a favored direction: we take advantage of the magnetic properties of the material to study its electric nonlinear properties, both seeming in a first step, completely distinct. The second-order polarization as well as the nonlinear electric susceptibility tensor of the material depend on the strength of the applied static magnetic field. This susceptibility tensor, characterizing the macrosystem, i.e., the magnetic fluid, is connected to the second-order polarizability tensor of an individual ferrite grain (microsystem) by statistical effects which depend on the particle volume fraction in the fluid and the volume of the grains.

The basis of our work is given by Kielich's model[9] for isotropic media containing molecules, with a permanent or induced static electric dipolar moment, immersed in a static electric field. In order to determine the orientation probability of the dipolar microsystems, the polarizability coefficients have to be calculated in the laboratory frame from those given in the microsystem axes and his model involves two angles θ and φ. This calculation is correct only if the microsystems which may be molecules but also more or less well-crystallized microstructures, have a symmetry of rotation around their electric dipolar moment. In the case of atoms or molecules of any shape, we must introduce a third angle ψ (θ, φ, and ψ being the Eulerian angles). This new possibility can let us hope to obtain a deeper knowledge of the microsystems and Kielich's results, which concern molecules having an axial symmetry, constitute a particular case in our calculation.

A. Langevin-like model

The magnetic fluid we use in our experiment is a suspension of magnetic dipolar particles. Each grain bears a macroscopic permanent magnetic moment $\boldsymbol{\mu}(|\boldsymbol{\mu}| \approx 10^4 \mu_B$, μ_B is Bohr's magneton). If a static magnetic field **B** is applied, the magnetic moments, submitted to thermal agitation, tend to rotate in order to align parallely to the field. We assume that the particles are rigid dipoles: the magnetic moments are linked to the grain crystalline lattices. The magnetic moment rotation makes the whole particle rotate and the second-order polarizability tensor is submitted to the same rotation operation.

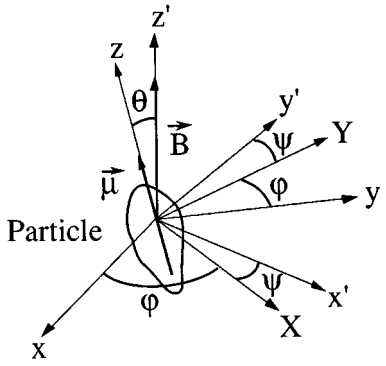

FIG. 1. Representation of the particle in the different referentials. The magnetic field B is applied along the z' axis and the particle magnetic moment is parallel to the z axis. X and Y are intermediate axes used in the rotation operation of the polarizability tensor from the particle axes (x,y,z) to the laboratory ones (x',y',z').

Let $\alpha^{2\omega}$ be the second-order polarizability tensor of one particle in the particle frame (x,y,z) and $\alpha'^{2\omega}$ the one in the laboratory frame (x',y',z') bound to **B**, as shown in Fig. 1. The transformation of this tensor is given by the following relation, using implicit summations:[21]

$$\alpha'^{2\omega}_{ijk}(\theta,\varphi,\psi)=a_{il}a_{jm}a_{kn}\alpha^{2\omega}_{lmn}, \tag{2}$$

where a_{ij} are the coefficients of the rotation matrix R^{-1} (θ,φ,ψ). θ, φ and ψ are the Eulerian angles which define the transformation R from the laboratory axes to the particle axes. This determination of $\alpha'^{2\omega}$ consists in a tedious calculation of 27 elements (or 18 by using contracted matrices). The polarizability tensor elements $\alpha^{2\omega}_{lmn}$ depend on the particle characteristics. The z' axis has been chosen along the direction of **B** and the z axis along the direction of $\boldsymbol{\mu}$ to simplify further calculations. The (x',y',z') frame is not, strictly speaking, a laboratory frame as the direction of **B** is sometimes changed in some experiments.

The macroscopic susceptibility tensor is given by the probability of finding a microsystem in the direction (θ,φ,ψ) and therefore of having $\alpha'^{2\omega}$ [Eq. (2)]. We suppose in a first approximation that the particles are monodisperse (magnetic moment of mean value μ) and that the magnetic fluid is diluted enough to neglect correlations between particles. This allows us to simply add the polarizability tensors in order to obtain the macroscopic susceptibility tensor d in the laboratory axes (the macroscopic electric field being supposed equal to the local one). If we make the assumption that all the particles have strictly identical properties, which is more restrictive than assuming the monodisperse property, we obtain

$$d_{ijk}=\frac{\Phi}{V}\langle\alpha'^{2\omega}_{ijk}\rangle_\Omega, \tag{3}$$

where Φ represents the particle volume fraction, V the volume of the particles. $\langle\alpha'^{2\omega}_{ijk}\rangle_\Omega$ is an average of $\alpha'^{2\omega}_{ijk}$, taking into account the probability of orientation of the particle in the elementary domain $d\Omega$ of the Eulerian angle space:

$$\langle\alpha'^{2\omega}_{ijk}\rangle_\Omega=\int_0^{2\pi}d\psi\int_0^{2\pi}d\varphi\int_0^{\pi}d\theta\,\sin\theta\,P(\theta,\varphi,\psi)\times\alpha'^{2\omega}_{ijk}(\theta,\varphi,\psi), \tag{4}$$

where $P(\theta,\varphi,\psi)$ is the orientation distribution function. This averaging is only orientational. The particles obey a Maxwell-Boltzmann distribution and therefore P depends only on θ by

$$P(\theta,\varphi,\psi)=\frac{1}{(2\pi)^2}P(\theta)=\frac{1}{(2\pi)^2}\frac{\exp(\mu B\cos\theta/kT)}{\int_0^{\pi}d\theta\,\sin\theta\,\exp(\mu B\cos\theta/kT)}$$

which ensures that $\int_0^{2\pi}d\psi\int_0^{2\pi}d\varphi\int_0^{\pi}d\theta\,\sin\theta\,P(\theta,\varphi,\psi)=1$. This function involves $(-\boldsymbol{\mu}\cdot\mathbf{B})$ the orientation energy of the magnetic particles and (kT) the thermal energy where k is the Boltzmann's constant and T the absolute temperature.

Our theory which is built on symmetryless and strictly identical particles could seem unrealistic. Our reasoning for the determination of the nonlinear susceptibility tensor of the medium can be seen as a modelization in which the nonlinear polarizability tensor of all the actual particles in the colloid is averaged in two main steps. In the first one, the averaging process is done on each tensor element by an integration on a size variable, the frames of reference being parallel for all the particles and fixed versus the magnetic moment and versus their crystal lattice. The second main step is the orientational averaging which is described all along this paper. This presentation in two independent steps is not perfectly rigorous because the orientational averaging [Eq. (4)] depends on particle size, via μ.

B. Symmetry of the poled MF for second-order phenomena

The third-rank tensors $\alpha^{2\omega}$ and $\alpha'^{2\omega}$ are written as contracted matrices. No assumption is made about the symmetry of the matrix $\alpha^{2\omega}$ characterizing the particle in its frame (C_1 point symmetry group). The only ''negative'' supposition is that the grain has no inversion symmetry to be able to exhibit a bulk second harmonic polarization. After the two first integrations of $\alpha'^{2\omega}_{im}$ on φ and ψ, only seven coefficients are nonzero, and four of them are independent; the new point symmetry group of the magnetic fluid under an applied field has a statistical origin:

$$\langle\alpha'^{2\omega}_{25}(\theta)\rangle_{\varphi,\psi}=\tfrac{1}{4}(3\cos^2\theta-1)(\alpha^{2\omega}_{25}-\alpha^{2\omega}_{14}),$$

$$\langle\alpha'^{2\omega}_{24}(\theta)\rangle_{\varphi,\psi}=\tfrac{1}{4}\{\cos^3\theta(\alpha^{2\omega}_{15}+\alpha^{2\omega}_{24})+(\cos\theta-\cos^3\theta)\times[-(\alpha^{2\omega}_{31}+\alpha^{2\omega}_{32})+2\alpha^{2\omega}_{33}]\},$$

$$\langle\alpha'^{2\omega}_{31}(\theta)\rangle_{\varphi,\psi}=\tfrac{1}{4}\{-2(\cos\theta-\cos^3\theta)[(\alpha^{2\omega}_{15}+\alpha^{2\omega}_{24})-\alpha^{2\omega}_{33}]+(\cos\theta+\cos^3\theta)(\alpha^{2\omega}_{31}+\alpha^{2\omega}_{32})\},$$

$$\langle \alpha'^{2\omega}_{33}(\theta)\rangle_{\varphi,\psi}=\cos^3\theta\alpha^{2\omega}_{33}+\tfrac{1}{2}(\cos\theta-\cos^3\theta)[2(\alpha^{2\omega}_{15}+\alpha^{2\omega}_{24})+(\alpha^{2\omega}_{31}+\alpha^{2\omega}_{32})],$$

and $\langle \alpha'^{2\omega}(\theta)\rangle_{\varphi,\psi}$ has the following form, according to Nye's notation:[21]

$$<\alpha'^{2\omega}(\theta)>_{\varphi,\psi}=\begin{pmatrix} \cdot & \cdot & \cdot & \circ\!\!\times & \cdot \\ \cdot & \cdot & \cdot & \bullet & \cdot \\ \bullet\!\!-\!\!\bullet & & \bullet & \cdot & \cdot \end{pmatrix} \tag{5}$$

where $(\cdot)$ represents a zero element, $(\bullet)$ a nonzero element; $(\bullet\!-\!\bullet)$ denotes two equal elements; $(\bullet\!-\!\circ)$ corresponds to equal elements but of opposite signs.

The orientational tensor averaging can be seen as a three-step process. The first one, an integration on ψ, is a rotational averaging around the magnetic moment $\boldsymbol{\mu}$. It provides a first step averaged polarizability tensor which exhibits a C_∞ symmetry around $\boldsymbol{\mu}$. We will call it ''intrinsic averaged polarizability tensor'' because in the averaging process, it is obtained at the last step where only intrinsic properties of the particles are taken into account. The second one, an integration on φ, is a rotational averaging around the magnetic field **B** of the first step averaged polarizability tensor. The result is a twice averaged polarizability tensor which exhibits a C_∞ symmetry around **B**. Lastly the third one, an integration on θ, brings the energetical aspect to the statistical average.

The $\langle \alpha'^{2\omega}(\theta)\rangle_{\varphi,\psi}$ matrix is obtained by an averaging process on a symmetryless particle which involves only proper rotations. Its symmetry must be searched among the point groups which leave the fluid invariant. The macrosystem has a symmetry of rotation around the applied field. There is no wonder that this matrix corresponds to the symmetry group C_∞. Notice that among crystallographic point groups, the hexagonal (C_6) and tetragonal (C_4) point groups give the same matrix. The $C_{\infty v}$ group would have been found if $\langle \alpha'^{2\omega}_{14}(\theta)\rangle_{\varphi,\psi}=-\langle \alpha'^{2\omega}_{25}(\theta)\rangle_{\varphi,\psi}=0$. But it cannot appear with a symmetryless particle because it would need improper rotations in the averaging process. If $\langle \alpha'^{2\omega}_{14}(\theta)\rangle_{\varphi,\psi}$ and $\langle \alpha'^{2\omega}_{25}(\theta)\rangle_{\varphi,\psi}$ which have opposite values [Eq. (5)] were found to be experimentally zero, it would be the sign of a certain symmetry in the polarizability tensor $\alpha^{2\omega}$ and in the particle, and conversely, experimental nonzero values of $\langle \alpha'^{2\omega}_{14}(\theta)\rangle_{\varphi,\psi}$ and of $\langle \alpha'^{2\omega}_{25}(\theta)\rangle_{\varphi,\psi}$ would prove a lack of symmetry of $\alpha^{2\omega}$ versus improper rotations, which is usually called chirality.

C. Field dependence of the MF nonlinear susceptibility

The integrations on θ of the four independent coefficients involve the first and second-order Langevin functions. We use Raikher and Shliomis's definition[17] for Langevin's functions: $L_0(a)=1$, $L_1(a)=\coth(a)-1/a$ (first order) and the higher-order functions are given by the following recurrence relation $L_{n-1}(a)-L_{n+1}(a)=[(2n+1)/a]L_n(a)$, which gives an orthogonal function set. For the second order, one obtains $L_2(a)=1-3\coth(a)/a+3/a^2$. The variable a is Langevin's parameter $\mu B/kT$. If a tends to zero, all these functions tend to zero and if a tends to infinity, their limit values are one. This definition is different from that of Kielich.[9] The independent nonzero elements $\langle \alpha'^{2\omega}_{im}\rangle_\Omega$ are then written as

$$\langle \alpha'^{2\omega}_{25}\rangle_\Omega=\frac{\alpha^{2\omega}_{25}-\alpha^{2\omega}_{14}}{2}L_2(a),$$

$$\langle \alpha'^{2\omega}_{24}\rangle_\Omega=\frac{\alpha^{2\omega}_{15}+\alpha^{2\omega}_{24}}{2}L_1(a)-\tilde{\alpha}^{\,2\omega}\frac{L_2(a)}{a},$$

$$\langle \alpha'^{2\omega}_{31}\rangle_\Omega=\frac{\alpha^{2\omega}_{31}+\alpha^{2\omega}_{32}}{2}L_1(a)-\tilde{\alpha}^{\,2\omega}\frac{L_2(a)}{a},$$

$$\langle \alpha'^{2\omega}_{33}\rangle_\Omega=\alpha^{2\omega}_{33}L_1(a)+2\tilde{\alpha}^{\,2\omega}\frac{L_2(a)}{a}, \tag{6}$$

with

$$\tilde{\alpha}^{\,2\omega}=\frac{2(\alpha^{2\omega}_{15}+\alpha^{2\omega}_{24})}{2}+\frac{\alpha^{2\omega}_{31}+\alpha^{2\omega}_{32}}{2}-\alpha^{2\omega}_{33}.$$

$L_2(a)/a$ is used in Eqs. (6) instead of $(1/5)[L_1(a)-L_3(a)]$ for the sake of simplicity. The response of the material is given by seven one-particle coefficients but only the four following independent combinations $(\alpha^{2\omega}_{25}-\alpha^{2\omega}_{14})$, $(\alpha^{2\omega}_{15}+\alpha^{2\omega}_{24})$, $(\alpha^{2\omega}_{31}+\alpha^{2\omega}_{32})$, and $\alpha^{2\omega}_{33}$ step in. As expected, the second-order polarizability terms tend to zero if the magnetic field tends to zero. The SH wave is generated in the magnetic fluid by orientation of the microsystems parallely to the field and cannot exist without it. It is worth noticing that $\langle \alpha'^{2\omega}_{25}\rangle_\Omega$ is an even function of **B** while the other averaged polarizability elements are odd ones. They depend on different symmetry properties of the intrinsic averaged polarizability tensor, as it will be commented later.

In the case of a very strong static magnetic field, the system tends to ''saturation.'' All the particle magnetic moments are aligned in the fluid ($\boldsymbol{\mu}$ and **B** parallel) and Eqs. (6) come down to the following simpler formulas:

$$\langle \alpha'^{2\omega}_{25}\rangle_{\Omega_{\rm sat}}=\tfrac{1}{2}(\alpha^{2\omega}_{25}-\alpha^{2\omega}_{14}),$$

$$\langle \alpha'^{2\omega}_{24}\rangle_{\Omega_{\rm sat}}=\tfrac{1}{2}(\alpha^{2\omega}_{15}+\alpha^{2\omega}_{24}),$$

$$\langle \alpha'^{2\omega}_{31}\rangle_{\Omega_{\rm sat}}=\tfrac{1}{2}(\alpha^{2\omega}_{31}+\alpha^{2\omega}_{32}),$$

$$\langle \alpha'^{2\omega}_{33}\rangle_{\Omega_{\rm sat}}=\alpha^{2\omega}_{33}. \tag{7}$$

It is not surprising to find that the asymptotic expressions of $\langle \alpha'^{2\omega}_{im}\rangle_\Omega$ are simply the averages of the particle polarizability elements $\alpha^{2\omega}_{im}$ over a 2π rotation around **B**. If particles have any shape, more precisely if they are not invariant under a rotation around $\boldsymbol{\mu}$, we have no means to get more information about them by a SHG experiment since we only have access to the following four global terms: $(\alpha^{2\omega}_{25}-\alpha^{2\omega}_{14})$, $(\alpha^{2\omega}_{15}+\alpha^{2\omega}_{24})$, $(\alpha^{2\omega}_{31}+\alpha^{2\omega}_{32})$, and $\alpha^{2\omega}_{33}$. We shall see later that they are experimentally nonzero. But all the other elements which are not mentionned could be zero without changing the result. In this case, the particles could exhibit some point symmetry groups, such as C_2, C_3, C_4, or C_6; the point symmetry groups C_n $(n\neq 2,3,4,6)$ and C_∞ are mathematically thinkable but they are very unlikely for a particle. The macrosymmetry (C_∞) necessarily differs from the microsymmetry since there is always a symmetry of revolution around the magnetic field in a magnetic fluid. Kielich asserted that the

macroscopic and the microscopic symmetries are identical[9] whereas, in a general model, the particle can have a smaller symmetry than the whole fluid.

Knowing the nonvanishing elements of the second-order electric susceptibility tensor [Eq. (5)], we are able to describe the SH macroscopic polarization vector in the magnetic fluid, for an incident laser beam at ω, whose electric field inside the magnetic fluid is noted $\mathbf{E}^{\omega}$:

$$P_{x'}^{2\omega}=2\frac{\Phi}{V}\left[-\langle\alpha'^{2\omega}_{25}\rangle_{\Omega}E_{y'}^{\omega}E_{z'}^{\omega}+\langle\alpha'^{2\omega}_{24}\rangle_{\Omega}E_{x'}^{\omega}E_{z'}^{\omega}\right],$$

$$P_{y'}^{2\omega}=2\frac{\Phi}{V}\left[\langle\alpha'^{2\omega}_{24}\rangle_{\Omega}E_{y'}^{\omega}E_{z'}^{\omega}+\langle\alpha'^{2\omega}_{25}\rangle_{\Omega}E_{x'}^{\omega}E_{z'}^{\omega}\right],$$

$$P_{z'}^{2\omega}=\frac{\Phi}{V}\left[\langle\alpha'^{2\omega}_{31}\rangle_{\Omega}[(E_{x'}^{\omega})^2+(E_{y'}^{\omega})^2]+\langle\alpha'^{2\omega}_{33}\rangle_{\Omega}(E_{z'}^{\omega})^2\right], \tag{8}$$

x',y',z' being the laboratory axes. A good choice of different configurations of the fundamental wave vector $\mathbf{k}_{\omega}$ and of the polarization direction $\mathbf{E}^{\omega}$ in the fluid with respect to $\mathbf{B}$ will help us to determine experimentally the values of various $\langle\alpha'^{2\omega}_{im}\rangle_{\Omega}$ elements as a function of B.

II. EXPERIMENTAL SETUP AND QUALITATIVE ASPECTS OF SHG

A. Experimental choices: Material and device

We use in our experiments a chemically synthesized magnetic fluid[16] based on cobalt ferrite particles ($CoFe_2O_4$), of mean diameter 14.1 nm (x-ray measurements), suspended in water. These compounds crystallize in the spinel structure[22,23] but the exact structure of the particle is more complicated.[24] They are magnetic monodomains and bear a permanent magnetic moment $\boldsymbol{\mu}$. The volume fraction Φ of the colloid is about 6%. The ratio between the magnetic anisotropy energy KV of the grain (K being the magnetic anisotropy constant,[25,26] V the volume of the microsystems) and the thermal energy kT is large: about 100 at room temperature, using the bulk K value. The high magnetic energy barrier KV prevents the magnetic moment from reversing without rotating the particle and this moment is thus linked to the grain crystalline frame.

The experimental setup is the following: a high peak power Nd:YAG laser provides picosecond pulses (80 ps, 125 kW at most) by packets (length 200 ns, repetition rate 1 kHz), of wavelength 1.064 μm. Its beam is focused onto a cell containing the magnetic fluid and submitted to a static magnetic field ranging from 0 to 0.3 T. SHG has been studied in transmission and we find that the best SH efficiency is provided by a 10-μm cell thickness because of strong absorption phenomena in magnetic fluids at 0.532 μm. The excitation power density is restricted to a very narrow range. The lower limit arises from SH detection possibilities and the upper one originates from the damage caused to the sample. The damage power density threshold and the optimized cell thickness will not be studied in this paper. The infinitesimal second harmonic generated signal is detected by a photomultiplier followed by a 20 dB amplifier, a boxcar-integrator and then an $x(t)$ recorder. In order to measure it, we have to get rid of the whole infrared power left and it is achieved by a second harmonic separator, placed just behind the sample, a visible filter and an interferential bandpass filter of $\Delta\lambda=1$ nm at 532 nm. The whole set has a 10^{-10} transmission rate for the IR beam and eliminates also radiations observed near 532 nm which are generated at 510–520 nm in the sample itself and may come from two-photon process luminescence.[27] Furthermore we take advantage of the poor quantum efficiency of the photomultiplier in the infrared range so that the measured electric current due to the infrared power left intensity can be weaker than the SH signal. This is in accordance with the very weak SH conversion efficiency found in the fourth part of this paper (about 10^{-13} times the incident infrared power). The SH signal is not very stable and this yields a relative error on the SH intensity measurements of about $\pm5\%$ in the best cases. It is caused by laser fluctuations and instabilities occurring inside the ferrofluid (mass transports induced by thermoconvection, thermodiffusion, and electrostriction).

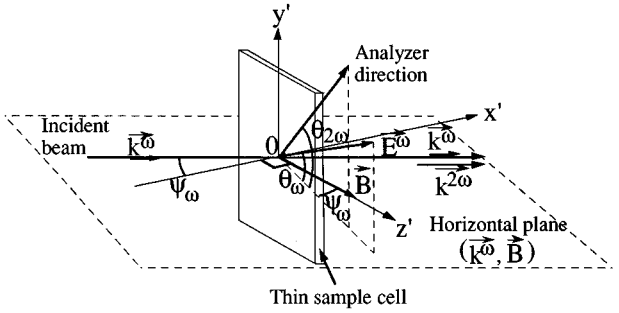

FIG. 2. Disposition of elements and notations.

In our experiment, the incident beam of wave vector $\mathbf{k}^{\omega}$ and the applied magnetic field $\mathbf{B}$ are both horizontal. The thin cell containing the sample is vertical and is kept in the $(y'Oz')$ plane, i.e., parallel to $\mathbf{B}$, to get rid of demagnetizing effects induced by the platelet cell shape. Let θ_{ω} and $\theta_{2\omega}$ be the angles between $\mathbf{B}$ and the polarization vector $\mathbf{E}^{\omega}$ of the incident beam and the SH beam analyzer direction, respectively. Let ψ_{ω} be the angle defining $\mathbf{k}^{\omega}$ in the $(x'Oz')$ horizontal plane (Fig. 2).

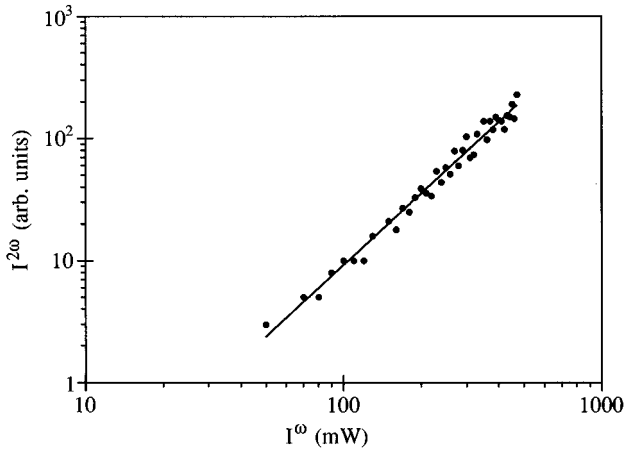

FIG. 3. Second harmonic generated intensity $I^{2\omega}$ vs mean incident intensity I^{ω}. The slope of the best-fit curve is equal to 2, proving a second-order nonlinear optical phenomenon. Experimental parameters are $B=0.3$ T, $S=0.5$ mm^2, $\theta_{\omega}=90°$, and $\psi_{\omega}=0°$.

B. Qualitative verifications of the model

Except for an unexpected but normal observation in which the SH beam is found not to be always linearly polarized [Fig. 6(b)], the qualitative foreseen aspects of the SHG are evidenced in Figs. 3, 4(a), and 4(b). We verify that we are in presence of a quadratic nonlinear effect since SH intensity is clearly proportional to the square of the incident light power, as shown in Fig. 3. In Figs. 4(a) and 4(b), our experimental results about SH intensity are presented as a function of the applied magnetic field strength in four different configurations for the directions of $\mathbf{B}$ and of $\mathbf{E}^{\omega}$. We also give in the same figures and for a better understanding, their best-fit curves, the determination of which will be explained further. Three of the configurations correspond to experiments made at $\psi_{\omega}=0°$ and $\theta_{\omega}=0°$, 45° or 90° [curves (A), (B), and (C)]; the fourth one is obtained by $\psi_{\omega}=40°$ and $\theta_{\omega}=0°$ [curve (D)]. With the different values used for $\theta_{2\omega}$, the actually measured bulk nonlinear coefficients are $\langle \alpha'^{2\omega}_{33}\rangle_{\Omega}$, $\langle \alpha'^{2\omega}_{24}\rangle_{\Omega}$, $\langle \alpha'^{2\omega}_{32}\rangle_{\Omega}$, and $\langle \alpha'^{2\omega}_{25}\rangle_{\Omega}$. From relations (5) between coefficients, these four configurations are sufficient to determine all the nonzero elements $\langle \alpha'^{2\omega}_{im}\rangle_{\Omega}$ of the bulk nonlinear susceptibility tensor of our model. Conversely, with $\theta_{\omega}=90°$, $\psi_{\omega}=0°$, and $\theta_{2\omega}=90°$ for instance, we find experimentally that the coefficient $\langle \alpha'^{2\omega}_{22}\rangle_{\Omega}$ is equal to zero as predicted. As put forward in the theoretical part, no frequency doubling is experimentally evidenced in the magnetic fluid when no magnetic field is applied (the electric dipolar approximation is justified) except in the tilted cell configuration as we will see few lignes further. The SH intensity increases with the magnetic field intensity. In all the four configurations, the bulk nonlinear electric susceptibility coefficients saturate for high magnetic fields (about 0.3 T), as qualitatively expected. These results are studied in detail in the fourth part of this paper.

C. Surface SHG effects

Actually, in curve (D) which corresponds to a tilted position of the cell ($\psi_{\omega}=40°$), we observe a signal at $B=0$ which does not arise from noise. At $B=0$, no bulk polarization $\mathbf{P}^{2\omega}(B=0)$ is expected in the limit of the electric dipole approximation. In the ''colloid-cell'' system the only places which do not exhibit any inversion symmetry, are the ''colloid-cell wall'' interfaces and a nonlinear surface polarization $\mathbf{P}_S^{2\omega}$ can appear on them.[2,28,29] As the fused silica cell walls have an amorphous glass structure, the minimal symmetry group of the ''colloid-cell wall'' system is C_{∞}. Larger groups, such as $C_{\infty v}$, which have C_{∞} as a subgroup, are also allowed; the experiment will determine to which symmetry group the ''colloid-cell wall'' system belongs. Surface polarization $\mathbf{P}_S^{2\omega}$ arises from particles adsorbed on the fused silica input and output faces. If thermal effects are neglected, their magnetic moments bound to their crystalline frames make with the cell normal $\mathbf{n}$ an angle θ which corresponds to a minimum in the interaction energy between particles and the glass surface. They are displayed in an $\mathbf{n}$-axis cone. Two limit cases are noticeable: if $\theta=0$ all the magnetic moments are parallel to $\mathbf{n}$ and if $\theta=90°$ they lay in the cell plane without any privileged orientation. The study of the collective behavior at finite temperature of particles at the interface is beyond the aim of this paper.

The nonzero coefficients of the surface nonlinear electric susceptibility tensor can be found by noticing a similarity between the orientating role of the cell wall normal on this surface tensor and that of an applied magnetic field on the bulk nonlinear electric susceptibility tensor. As $\mathbf{n}$ is parallel to the (Ox') axis in the laboratory frame (Fig. 2), the surface nonlinear electric susceptibility contracted matrix can be written with the same notations as in Eq. (5):

$$<\alpha'^{2\omega}_{S}>_{\Omega'}=\begin{pmatrix} \blacktriangle & \blacktriangle\!\!-\!\!\blacktriangle & . & . & . \\ . & . & . & . & \triangle\!\!\times\!\!\blacktriangle \\ . & . & . & . & \blacktriangle\!\!\times\!\!\blacktriangle \end{pmatrix} \tag{9}$$

Ω' being a solid angle around $\mathbf{n}$, analogous to Ω for the bulk contribution. In the case of a $C_{\infty v}$ symmetry of the two-dimensional system, $\langle \alpha'^{2\omega}_{S\,25}\rangle_{\Omega'}$ and $\langle \alpha'^{2\omega}_{S\,36}\rangle_{\Omega'}$ would be zero. The nonzero surface nonlinear terms are only seen in tilted configurations ($E^{\omega}_{x'}\neq 0$ or $P^{2\omega}_{x'}\neq 0$). Some of the nonzero surface nonlinear terms cannot be obtained with our actual experimental setup (Fig. 2). Let $\mathbf{n}_{\text{in}}$ and $\mathbf{n}_{\text{out}}=-\mathbf{n}_{\text{in}}$ be the normals to the input and output faces pointing outside the cell. The ''colloid-output wall'' system is obtained from the ''colloid-input wall'' system by a rotation of π. This is equivalent to rotate the incident electric field $\mathbf{E}^{\omega}$ and the surface polarization vector $\mathbf{P}_S^{2\omega}$ of π around the y' direction (Fig. 2) and it leads to the following relation:

$$\langle \alpha'^{2\omega}_{S\,25}\rangle_{\Omega'\ \text{input}}=\langle \alpha'^{2\omega}_{S\,25}\rangle_{\Omega'\ \text{output}}.$$

$\langle \alpha'^{2\omega}_{S\,25}\rangle_{\Omega'}$ is an even function of $\mathbf{n}$. Phase mismatch between output and input 2ω generated waves is about π for a 10-μm cell thickness with $n^{\omega}-n^{2\omega}=0.028$ (Appendix A) but $\mathbf{P}^{2\omega}_{S\ \text{input}}$ contribution can be neglected because of the large absorption coefficient of the medium at 2ω.

Particle orientation near the surface is necessarily affected by applying a static magnetic field. Magnetic grains cannot be pulled out of the surface because the magnetic field gradient at the interface is not large enough in our experiment, but surface polarization $\mathbf{P}_S^{2\omega}$ is necessarily modified by B as well as, in return, bulk polarization $\mathbf{P}^{2\omega}(B)$ is influenced by a change in $\mathbf{P}_S^{2\omega}$. We assume that these effects are small and we will consider that $\mathbf{P}_S^{2\omega}$ does not depend on B and that further calculations on bulk nonlinear coefficients are not modified by $\mathbf{P}_S^{2\omega}$. In our model it means that the volume fraction may be modified by an adsorption phenomenon but does not change with B. For clarity and in spite of their different nature, we represent the sum of bulk and of surface contributions in the same contracted matrix with circles and triangles, respectively:

$$<\alpha'^{2\omega}_{\text{Total}}>=\begin{pmatrix} \blacktriangle & \blacktriangle\!\!-\!\!\blacktriangle & \circ\!\!\bullet & . \\ . & . & . & \triangle\!\!\times\!\!\blacktriangle \\ \bullet\!\!-\!\!\bullet & \bullet & . & \blacktriangle\!\!\times\!\!\blacktriangle \end{pmatrix} \qquad [(5)+(9)].$$

The only nonlinear term common to both phenomena is $\langle \alpha'^{2\omega}_{\text{Total}\,25}\rangle$ and it is in fact the element for which we have experimentally evidenced a nonlinear contribution at $B=0$ [measurement for a tilted cell at $\theta_{\omega}=0°$ and $\psi_{\omega}=40°$ pre-

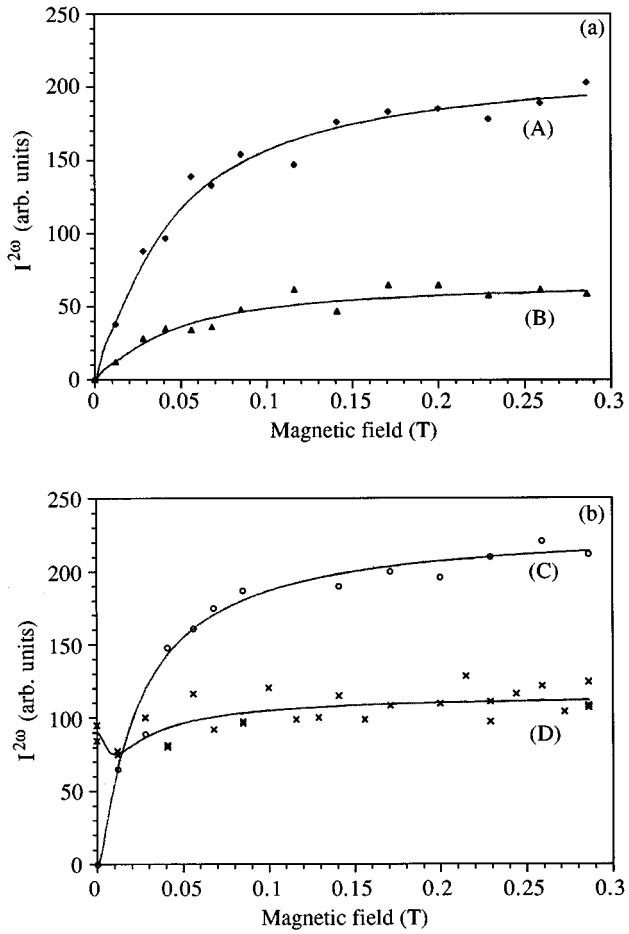

FIG. 4. (a) and (b) Second harmonic generated intensity vs B for all the four independent ($\mathbf{E}^{\omega}$,$\mathbf{B}$) direction configurations.

$$\left.\begin{array}{ll}(A) & \blacklozenge,\ \theta_{\omega}=\theta_{2\omega}=0°,\\ (B) & \blacktriangle,\ \theta_{\omega}=45°,\ \theta_{2\omega}=90°,\\ (C) & \bigcirc,\ \theta_{\omega}=90°,\ \theta_{2\omega}=0°,\end{array}\right\}\ \psi_{\omega}=0°,$$
$$(D)\quad \times,\ \theta_{\omega}=0°,\ \theta_{2\omega}=90°,\ \psi_{\omega}=40°.$$

The plots correspond to the measured intensity $I^{2\omega}$ under normal incidence [curves (A), (B) and (C)] and to $I^{2\omega}$ divided by the factor $(2\cos\psi_{\omega}\sin\psi_{\omega})^2$ [Eq. (B3)] under oblique one [curve (D)]. In the latter case, the detected intensity is very small but is divided by a weak factor. For a better understanding, experimental data are presented together with the best-fit curves, calculated with an effective magnetic field taking into account the magnetic interactions between particles.

sented in Fig. 4(b)]. It is the reason why SHG at $B=0$ has not been seen in three configurations among four [Figs. 4(a) and 4(b)]. Reciprocally the observed lack of SHG at any B in geometries which correspond to zero elements of $\langle\alpha'^{2\omega}_{\text{Total}}\rangle$ proves that nonlinear combinations of surface and volume particle orientations are negligible.

After a first assumption about the constancy of $P_S^{2\omega}$ versus B, we can try to find a link between $P_S^{2\omega}$ and the nonlinear bulk polarization. As we have already assumed that $\mathbf{n}_{\text{out}}$ plays the same orientating role for surface SHG as $\mathbf{B}$ for the bulk one, tensors are similar for both phenomena. As the bulk SH polarization y' component is given by

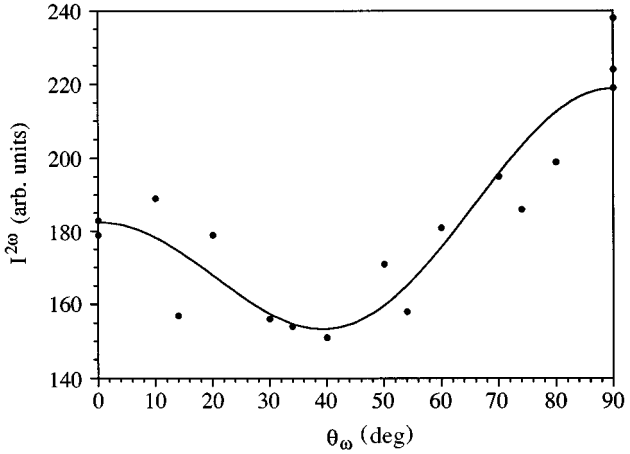

FIG. 5. Second harmonic generated intensity $I^{2\omega}$ for different incident polarization directions in the configuration $\psi_{\omega}=0°$ and for an applied magnetic field of 0.15 T. Experimental data and the best-fit curve are presented.

$$P_{y'}^{2\omega}(B)=\langle\alpha'^{2\omega}_{25}(B)\rangle_{\Omega}\,\frac{(E_{\text{in}}^{\omega})^2}{2}\sin 2\psi_{\omega},$$

E_{in}^{ω} being the real amplitude in vacuum of the input fundamental electromagnetic field, its corresponding output surface component is obtained from $\mathbf{P}_{y'}^{2\omega}$ by a rotation of $\pi/2$ around y' for a particular value B_0 of B, where B_0 is a virtual magnetic field corresponding to the particle binding energy to the glass wall:

$$P_{S\,y',\,\text{output}}^{2\omega}=\kappa\langle\alpha'^{2\omega}_{25}(B_0)\rangle_{\Omega}\,\frac{(E_{\text{in}}^{\omega})^2}{2}\sin 2\left(\psi_{\omega}+\frac{\pi}{2}\right).$$

κ is a length dimensioned constant which can be seen as the ratio of a surface particle concentration and of a volume particle concentration. If, as assumed, particles orientated by $\mathbf{B}$ and by $\mathbf{n}_{\text{out}}$ had the same characteristics, κ should be a positive constant and this would lead to a substractive effect because of the angle $\pi/2$ in the above expression. Complex bulk and surface contributions are summed in the output generated SH electromagnetic wave amplitude $E_{\text{out}\,y'}^{2\omega}$. Let H_{oblique} be the complex proportionality coefficient for the bulk contribution (Appendix B) and H_S be the similar coefficient for the surface contribution in $E_{\text{out}\,y'}^{2\omega}$ which can be written as

$$E_{\text{out}\,y'}^{2\omega}=[H_{\text{oblique}}\langle\alpha'^{2\omega}_{25}(B)\rangle_{\Omega}-\kappa H_S\langle\alpha'^{2\omega}_{25}(B_0)\rangle_{\Omega}]\,\frac{\Phi(E_{\text{in}}^{\omega})^2}{2V\varepsilon_0}\sin 2\psi_{\omega}. \quad (10)$$

This wall orientation hypothesis will be compared with the experimental results.

D. Magnetic particle and magnetic fluid symmetries

The uncertainty about the bulk contribution corresponding to the $\langle\alpha'^{2\omega}_{25}\rangle_{\Omega}$ term in curve (D), is large but this term is undeniably nonzero. The fact that $\langle\alpha'^{2\omega}_{S\,25}\rangle_{\Omega'}$ is also nonzero proves that the magnetic fluid symmetry is not $C_{\infty v}$ but C_{∞} if the colloid is orientated by a glass cell wall. Surface and bulk

SH analyses converge to establish that ferrofluids, whose particles are orientated in a favored direction, are invariant under a C_∞ symmetry group without any reflection plane invariance. This agrees with our model in which no assumption is made about particle symmetry properties. From Eq. (6), it simply proves that $\alpha_{14}^{2\omega} \neq \alpha_{25}^{2\omega}$: in the case of a C_n symmetry of the particle, the C_{nv} symmetry is not observed. If the particle has no particular symmetry ($n=1$), one can see it as a rock for instance.

The Kleinman conjecture[30] which applies only for lossless media, would provide additional relations between polarizability tensor elements and for $\alpha'^{2\omega}_{25}$, we would have

$$\alpha'^{2\omega}_{14} = \alpha'^{2\omega}_{25} = \alpha'^{2\omega}_{36}.$$

These relations, joined to those arising from the C_∞ symmetry [Eq. (5)] of the medium, would imply that

$$\langle \alpha'^{2\omega}_{14} \rangle_\Omega = \langle \alpha'^{2\omega}_{25} \rangle_\Omega = \langle \alpha'^{2\omega}_{36} \rangle_\Omega = 0.$$

Therefore the C_∞ symmetry of a medium can be distinguished from a $C_{\infty v}$ symmetry by SHG measurements only in the case of a strong optical absorption. It is the case of our ferrofluid at $\lambda = 532$ nm.

III. BULK SHG MACROSCOPIC ANALYSIS

In a first step, our model can be tested in its macroscopic symmetry aspects. More precisely, the SH intensity measured in geometries in which only bulk effects take place, is compared to formulas arising from Eq. (5). The symmetry of the system can be proved and numerical relations between some of the d_{im} elements can be evaluated and then compared to values given by the statistical study in the fourth part of the paper.

A. SH intensity analysis as a function of input polarization direction

Two kinds of experiments are done: in both, the incident beam direction is perpendicular to the cell plane ($\psi_\omega = 0°$) and the applied magnetic field strength is fixed. In the first one ($B = 0.15$ T), the SH intensity is measured without analyzer, by varying the angle θ_ω between the incident wave polarization direction and the applied field, as it is shown in Fig. 5. Using Eqs. (A1), (A3), (A6) of Appendix A and the definition relations $I_{\text{in}}^{\omega} = (1/2) S \varepsilon_0 c |E_{\text{in}}^{\omega}|^2$ and $I_{\text{out}}^{2\omega} = (1/2) S \varepsilon_0 c |E_{\text{out}}^{2\omega}|^2$ for the input and output powers in vacuum at ω and 2ω, the second harmonic generated power measured at the output of the cell for $\psi_\omega = 0$ is written as

$$I_{\text{out}}^{2\omega}(\theta_\omega, 0) = \frac{2 (I_{\text{in}}^{\omega})^2}{S \varepsilon_0 c} \left\{ \left| \frac{D_{24}}{\varepsilon_0} \right|^2 \sin^2 2\theta_\omega + \left| \frac{D_{32}}{\varepsilon_0} \sin^2 \theta_\omega + \frac{D_{33}}{\varepsilon_0} \cos^2 \theta_\omega \right|^2 \right\}.$$

S is the laser beam cross section in the sample, ε_0 is the vacuum permittivity, and c is the light velocity. The complex terms D_{im} are defined as the product of d_{im} and of H_{ijk}, the latter accounting for the Fabry-Perot effects in the sample, magnetic field birefringence and dichroism effects for the different configurations of polarization (see Appendix A). Complex factors H_{ijk} do not depend very much on i,j,k and on the magnetic field strength (Appendix A). They can be factorized in the above expression so that the nonlinear susceptibility d will be used further instead of the effective one D. As it will be seen further, our experiments lead us to take d_{im} terms as complex quantities which is often forgotten because it is rarely proved. As our setup exhibits a slightly different response at 2ω for vertical and horizontal polarizations, the measured intensity takes the following form with the experimental transmission factor $g = 0.75$:

$$I_{\text{mes}}^{2\omega}(\theta_\omega, 0) = \frac{2 (I_{\text{in}}^{\omega})^2}{S \varepsilon_0 c} |H|^2 \left\{ \left| \frac{d_{24}}{\varepsilon_0} \right|^2 g \sin^2 2\theta_\omega + \left| \frac{d_{32}}{\varepsilon_0} \sin^2 \theta_\omega + \frac{d_{33}}{\varepsilon_0} \cos^2 \theta_\omega \right|^2 \right\}. \quad (11)$$

The least-squares-fit value found for $|d_{33}/d_{32}|$ is 0.91 ± 0.04 at 0.15 T and the phase difference δ between d_{32} and d_{33} obeys to ($\delta > 56.6°$). Both results can be compared with those obtained by the statistical study in the fourth part of the paper which are $|d_{33}/d_{32}| = 0.93 \pm 0.02$ and $\delta = 147°$ which is indeed larger than 56.6°.

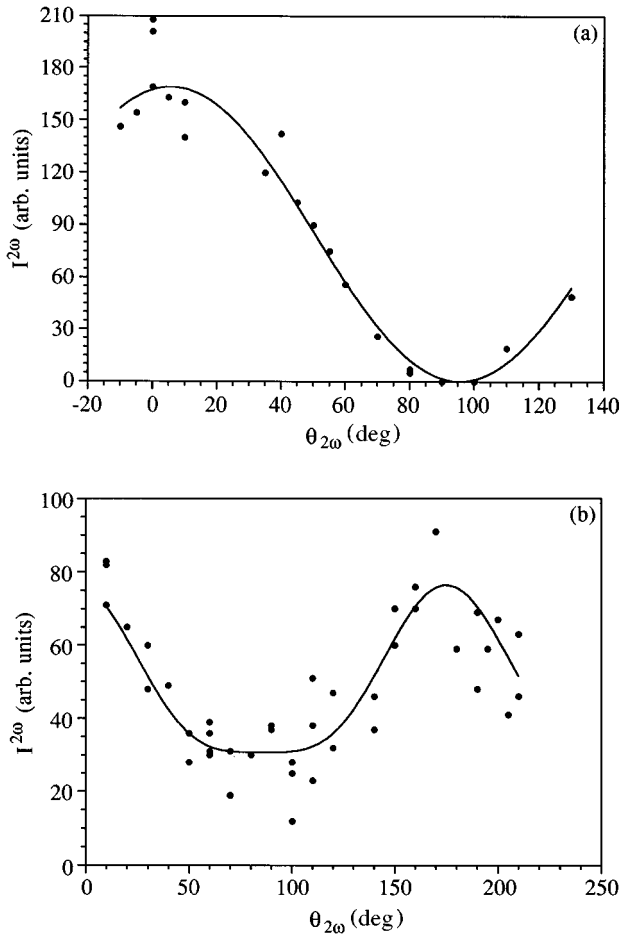

FIG. 6. (a) and (b) Polarization analysis of the second harmonic generated intensity $I^{2\omega}$ in two configurations: (a) $\theta_\omega = 90°$ and (b) $\theta_\omega = 45°$. $\theta_{2\omega}$ is the analyzer direction with respect to the horizontal plane. The applied magnetic field is 0.2 T.

B. Ellipticity of the generated SH wave

In the second series of experiments of this macroscopic analysis, the SH intensity is measured as a function of the analyzer direction $\theta_{2\omega}$ for a fixed polarization direction θ_ω of the fundamental wave and a fixed magnetic field strength ($B=0.2$ T). At $\theta_\omega=0°$ and $\theta_\omega=90°$ [Fig. 6(a)], the SH wave is linearly polarized parallel to z' [Eq. (8)]. For an oblique polarization direction at ω ($\theta_\omega=45°$ here), a SH vertical component due to d_{24} appears which is not in phase with the d_{32} and d_{33} horizontal one. No wonder that an elliptic polarization be clearly found [see Fig. 6(b)]. The output SH intensity takes into account three different angles: θ_ω and $\theta_{2\omega}$ which are already defined (Fig. 2) and β which expresses the slight lack of horizontality of **B** due to its nonhomogeneity between polar pieces. The measured SH intensity is written as [Eq. (8)]:

$$I^{2\omega}_{\rm mes}(\theta_\omega,\psi_\omega=0,\beta,\theta_{2\omega})\approx(g\ \cos^2\theta_{2\omega}+\sin^2\theta_{2\omega})|(D_{32}\sin^2\theta_\omega+D_{33}\cos^2\theta_\omega)\cos(\theta_{2\omega}-\beta)+D_{24}\sin 2\theta_\omega\sin(\theta_{2\omega}-\beta)|^2.$$

It can be identified to a Fourier expansion on $\theta_{2\omega}$:

$$I^{2\omega}_{\rm mes}=a+b\ \cos2(\theta_{2\omega}+\varphi_1)+c\ \cos4(\theta_{2\omega}+\varphi_2).$$

The lack of horizontality of **B** is critical in this experiment because the analyzer is rotated at the sample output. It has not to be considered in the other experiments [Figs. 4(a), 4(b) and 5] since a 7° slope of **B** gives only a 1.5% admixture between the d_{32} and d_{33} contributions [Eq. (11)]. The values of a/b and φ_1 are obtained by least-squares fits on the Fourier expansion of the experimental $I^{2\omega}_{\rm mes}$ curves [partially presented in Figs. 6(a) and 6(b)]. They are given in Table I for three experiments in which the parameter $(\theta_\omega+\beta)$, the really measured angle, is equal to 0°, 45°, or 90°. The quantities c and φ_2 are not given here since they give a weak imprecise contribution in the fitting.

The ratios a/b and the angles φ_1 are also calculated at 0.2 T for $\theta_\omega+\beta=0°$, 45°, and 90°, with the values of $\alpha^{2\omega}_{im}$ found by the statistical study in the fourth part of the paper [Eq. (12a)]. The macroscopic and the statistical studies give exactly the same results in the three configurations with a lack of horizontality of $\beta\approx7°$. The comparison between these two methods are led more precisely for $\theta_\omega+\beta=45°$ because in this geometry SH polarization is elliptic and the relative phases of three complex polarizability tensor elements play an important role. In this configuration, the values found for a/b and φ_1 are used to adjust [Eq. (12b)] the values of $\alpha^{2\omega}_{im}$ given in Eq. (12a) within their uncertainty range. This enhanced precision comes from the complementarity of the two measurements. Experimental values of a/b, φ_1, and β ($\beta=7.2°\pm0.3°$) are found with a global accuracy of 0.5%. The y' and the z' components of the SH electric fields at 0.2 T are found to be dephased of an angle $\delta'=79.2°$. This phase difference cannot arise only from the MF optical birefringence contribution:[31] with the 10-μm-thick cell, an approximative birefringence of 5×10^{-3} for the sample used at 0.2 T gives at most a dephasing angle of $\pm34°$ (its sign being still unknown). Then one must consider the $d_{\rm im}$ terms as complex values. The determination of $|d_{25}|$ with respect to the other elements is not already done because it needs a continuous variation of ψ_ω which is difficult to achieve with our experimental device.

TABLE I. Values of the parameters a/b and φ_1 determined by least-squares fits of three experiments of polarization analysis. Two among three of these experiments are presented in Figs. 6(a) and 6(b) with their least-squares fits on a second-order limited Fourier expansion.

$\theta_\omega+\beta$	φ_1	a/b-SH polarization
0°	−10.83°	≈1-almost linear
45°	5.00°	2.10-elliptic
90°	−5.56°	≈1-almost linear

IV. VALIDITY OF THE STATISTICAL MODEL AND DETERMINATION OF THE SECOND-ORDER POLARIZABILITY TENSOR COEFFICIENTS OF AN INDIVIDUAL FERRITE GRAIN

A. Relative determination of the extended Langevin-like model parameters

After this macroscopic study, we can, with our statistical model, get information about the individual particles suspended in the fluid, which is the main goal of this paper. There are two possibilities to obtain the values of the second-order polarizability tensor coefficients for one particle: the first one by considering the nonlinear effects at saturation; the second one by verifying the theoretical laws implying Langevin's functions, through their fitting to the experimental results shown in Figs. 4(a) and 4(b).

If the fluid is submitted to a high magnetic field, all the grains tend to align parallely to the field and, by selecting input polarizer and output analyzer directions, we have a direct access to the moduli of the three nonlinear coefficients of the particle [global terms $(\alpha^{2\omega}_{15}+\alpha^{2\omega}_{24})$, $(\alpha^{2\omega}_{31}+\alpha^{2\omega}_{32})$, and $\alpha^{2\omega}_{33}$] according to Eqs. (7). These values are determined by the saturation level of curves (A, B, and C, respectively) shown in Figs. 4(a) and 4(b). The direct determination of $(\alpha^{2\omega}_{25}-\alpha^{2\omega}_{14})$ from the saturation level in curve (D) cannot be made because the surface polarization $\mathbf{P}^{2\omega}_S$ must be taken into account and is not known with this method. In our device the highest homogeneous magnetic field we can apply is 0.3 T and we will suppose, in this first step, that the values measured at 0.3 T are saturation ones. Results are given in arbitrary units, which accounts for the coefficient $[2(I^\omega_{\rm in})^2\Phi^2/S\varepsilon_0cV^2]|H|^2$ coming from Eqs. (3) and (11) and for the detection device gain. An error of 5% has been taken into account on the SH intensity values which gives a 2.5% error on the three following amplitude-type terms:

$$\tfrac{1}{2}|\alpha_{15}^{2\omega}+\alpha_{24}^{2\omega}|=0.46\pm0.01 \text{ arb. units},$$
$$\tfrac{1}{2}|\alpha_{31}^{2\omega}+\alpha_{32}^{2\omega}|=1.00\pm0.02 \text{ arb. units},$$
$$|\alpha_{33}^{2\omega}|=0.98\pm0.02 \text{ arb. units}.$$

A better method consists in comparing the complete experimental data set, obtained for all values of the applied magnetic field strength [Figs. 4(a) and 4(b)], with the theoretical curves given by Eqs. (3), (6), (A4), (A6), and (11) under normal incidence (see Appendix A) and Eqs. (3), (6), (B3), (B4), and (B5) under oblique one (see Appendix B). In this case, Eq. (6) must be modified to include the constant surface contribution $\langle \alpha'^{2\omega}_{S\,25}\rangle_{\Omega'}$ which has already been discussed:

$$\langle \alpha'^{2\omega}_{25}\rangle_{\Omega}=\tfrac{1}{2}(\alpha_{25}^{2\omega}-\alpha_{14}^{2\omega})L_2(a)+\langle \alpha'^{2\omega}_{S\,25}\rangle_{\Omega'}$$

with $a=\mu B/kT$. This complete comparison is more reliable than using measures made at a doubtful saturation level. This is achieved by fitting simultaneously four different functions to the experimental data given in the four curves (A), (B), (C), and (D) shown in Figs. 4(a) and 4(b). This global fitting, done according to the nonlinear Levenberg-Marquardt method, is needed by the fact that some parameters appear simultaneously in different functions to be fitted. It is also an opportunity for finding complex values of the $\alpha_{\text{im}}^{2\omega}$ parameters, one of them being arbitrarily chosen as real, and for bringing a great precision into the final results. As the $(1/2)(\alpha_{25}^{2\omega}-\alpha_{14}^{2\omega})$ parameter is only coupled to $\langle \alpha'^{2\omega}_{S\,25}\rangle_{\Omega'}$ and vice versa, $\langle \alpha'^{2\omega}_{S\,25}\rangle_{\Omega'}$ can also be chosen as real. The following nine parameters have to be determined, the real and imaginary parts of $(1/2)(\alpha_{25}^{2\omega}-\alpha_{14}^{2\omega})$, of $(1/2)\langle\alpha_{15}^{2\omega}+\alpha_{24}^{2\omega})$ and of $\alpha_{33}^{2\omega}$, the real parts of $(1/2)(\alpha_{31}^{2\omega}+\alpha_{32}^{2\omega})$ and of $\langle \alpha'^{2\omega}_{S\,25}\rangle_{\Omega'}$ (their imaginary parts being zero by hypothesis) and μ/kT. The first seven parameters are weights for Langevin's functions $L_1(\mu B/kT)$ and $L_2(\mu B/kT)$ and the last one is Langevin's parameter divided by B. An additional parameter g accounts for the different transmission factors of the second harmonic separator according to the SH polarization directions (it concerns the transmission factors of the experimental device, external to the nonlinear material). The same $\pm5\%$ error is estimated on the SH intensity data for the fitting. The very good agreement between the four theoretical curves and their corresponding data set proves the validity of our Langevin-like model. The cobalt ferrite particles used in our experiment are then characterized by

$$\langle \alpha'^{2\omega}_{S\,25}\rangle_{\Omega'}=(0.67\pm0.03) \text{ arb. units},$$
$$\tfrac{1}{2}(\alpha_{25}^{2\omega}-\alpha_{14}^{2\omega})=(0.72\pm0.10)e^{\pm i(1.99\pm0.17)} \text{ arb. units},$$
$$\tfrac{1}{2}(\alpha_{15}^{2\omega}+\alpha_{24}^{2\omega})=(0.49\pm0.02)e^{i(0.52\pm0.04)} \text{ arb. units},$$
$$\tfrac{1}{2}(\alpha_{31}^{2\omega}+\alpha_{32}^{2\omega})=(1.04\pm0.10) \text{ arb. units},$$
$$\alpha_{33}^{2\omega}=(1.02\pm0.04)e^{i(2.61\pm0.05)} \text{ arb. units}. \quad (12a)$$

These results are actually obtained by an effective magnetic field model[32] which will be presented at the same time as the value found for μ/kT since it depends strongly on this correction whereas the $\alpha_{\text{im}}^{2\omega}$ coefficients are almost not affected by it. A more precise determination of the last three terms given in Eqs. (12a) within their uncertainty range is made by comparing these results to those obtained by a polarization analysis [Fig. 6(b)] and it gives

$$\tfrac{1}{2}(\alpha_{15}^{2\omega}+\alpha_{24}^{2\omega})=0.51e^{i0.52} \text{ arb. units},$$
$$\tfrac{1}{2}(\alpha_{31}^{2\omega}+\alpha_{32}^{2\omega})=1.01 \text{ arb. units},$$
$$\alpha_{33}^{2\omega}=1.01e^{i2.61} \text{ arb. units}. \quad (12b)$$

Two comments can be brought about the first two values found in Eq. (12a). First the phase sign of $(1/2)(\alpha_{25}^{2\omega}-\alpha_{14}^{2\omega})$ remains undetermined by our technique. Second an identification of the modified expression of $\langle \alpha'^{2\omega}_{25}\rangle_{\Omega}$ with that given by our wall orientated model for surface SHG and expressed by Eq. (10), implies that

$$\frac{\langle \alpha'^{2\omega}_{S\,25}\rangle_{\Omega'}}{(1/2)(\alpha_{25}^{2\omega}-\alpha_{14}^{2\omega})}=-\frac{\kappa H_S}{H_{\text{oblique}}}L_2(a_0)$$

with $a_0=\mu B_0/kT$. H_S, H_{oblique}, κ, and a_0 are dimensionless quantities. In this relation κ and a_0 are unknown but there is a relation between the phases of the different elements, κ and $L_2(a_0)$ being real. H_{oblique} is defined in Appendix B and its phase Φ_B is equal to $0.454\times2\pi$ rad. A formulation of H_S can be made from Ref. 29 by taking the cell thickness (10 μm) and the phase mismatch (see Appendix A) into account. When SHG arises only from the cell output face, its phase Φ_S is equal to $-1.783\times2\pi$ rad. If Eq. (10) is valid, $(\Phi_S-\Phi_B+\pi\pm1.99)/2\pi$ should be an integer [the value 1.99 coming from Eq. (12a)]. Effectively we find $-1.783-0.454+0.5-1.99/2\pi=-2.054$, which is a mark in favor of our hypothesis in which the cell normal plays a role similar to that of a magnetic field.

B. Absolute evaluation of the nonlinear coefficients

The SH intensity generated in the ferrofluid under magnetic field is too weak to be measured with a power meter and using a photomultiplier is necessary. In order to obtain values in SI units for the macroscopic nonlinear coefficients $\langle \alpha'^{2\omega}_{\text{im}}\rangle_{\Omega}$ we use a calibrated 482-μm-thick bulk GaP sample oriented normally to the $\langle 111\rangle$ direction, of effective coefficient $d_{\text{eff GaP}}/\varepsilon_0=2/\sqrt{6}\times1.0\times10^{-10}m\ V^{-1}$ at 1.318 μm.[33] This sample is adequate for a comparison since its absorption coefficients at 532 nm and 1.06 μm are comparable to those of our magnetic fluid. Let $I_{\text{out sat}}^{2\omega}$ be the measured SH intensity for the magnetic fluid sample and $I'^{2\omega}_{\text{out}}$ for the GaP one. For the magnetic fluid sample, the experiment is done under a 0.3-T field considered for simplicity as the saturation level, and for $\theta_\omega=90°$ and $\psi_\omega=0°$. These measurements are very imprecise for both materials and lead to the ratio

$$\frac{I_{\text{out sat}}^{2\omega}}{I'^{2\omega}_{\text{out}}}=(1.14\pm0.42)\times10^{-5} \quad (13)$$

and from Eqs. (A5), (A6), and (11), we have

$$\frac{d_{32_{\text{sat}}}}{d_{\text{eff Gap}}}=\sqrt{\frac{F'}{|H|^2}\frac{I_{\text{out sat}}^{2\omega}}{I'^{2\omega}_{\text{out}}}}. \quad (14)$$

The dimensionless F' factor, accounting for the Fabry-Perot effects in the GaP sample, is already known from Ref. 33 ($F'=0.0061$); the value $|H|^2=8.60$ concerns the MF sample contained in the fused silica cell and is proportional to F (analogous factor for the ferrofluid to the factor F', defined for GaP, see Appendix A). $|H|^2$ is larger than F' because the refractive indices at ω and 2ω are very close to each other in our magnetic fluid. The SH susceptibilities of the magnetic fluid determined from Eqs. (3), (6), (12a), (13), and (14) are

$$\left|\frac{d_{25_{\text{sat}}}}{\varepsilon_0}\right|=(3.85\pm1.99)\times10^{-15}\ \text{m V}^{-1},$$

$$\frac{d_{32_{\text{sat}}}}{\varepsilon_0}=(5.59\pm2.06)\times10^{-15}\ \text{m V}^{-1},$$

$$\frac{d_{24_{\text{sat}}}}{\varepsilon_0}=(2.64\pm1.29)\times10^{-15}e^{i(0.52\pm0.04)}\ \text{m V}^{-1},$$

$$\frac{d_{33_{\text{sat}}}}{\varepsilon_0}=(5.45\pm2.73)\times10^{-15}e^{i(2.61\pm0.05)}\ \text{m V}^{-1}. \quad (15)$$

An effective nonlinear coefficient of the bulk material can be defined as $d_{\text{im bulk}}=d_{\text{im}}/\Phi$. For instance, the $d_{32\ \text{bulk}_{\text{sat}}}$ value can be compared to that of $d_{\text{eff GaP}}$ from Eq. (14) and with $\Phi=6\%$:

$$d_{32\ \text{bulk}_{\text{sat}}}=(1.1\pm0.4)\times10^{-3}\times d_{\text{eff Gap}}.$$

The d_{32} bulk value, at the saturation and in the limit $\Phi=1$, corresponds to an almost ''dry magnetic fluid'' and is not very far from that of many well-known SH generating crystals. For example, the nonlinear coefficient d' of KH_2PO_4 (KDP) (Ref. 33) is only about six times larger than the d_{32} bulk one at saturation [Eq. (15)].

In spite of the d_{32} bulk value, the actually measured SH intensity is very small. Considering the term $d_{32_{\text{sat}}}$ directly determined from Eqs. (13) and (14), the conversion efficiency in vacuum and at the saturation level, defined as $\rho_{\text{sat}}=I^{2\omega}_{\text{out sat}}/I^{\omega}_{\text{in}}$, is given by Eq. (25) in Ref. 33 and Eq. (A5):

$$\rho_{\text{sat}}=\frac{2I^{\omega}_{\text{in}}}{S\varepsilon_0 c}\left(\frac{d_{32_{\text{sat}}}}{\varepsilon_0}\right)^2|H|^2=2.2\times10^{-13},$$

where I^{ω}_{in} is the peak power at ω ($I^{\omega}_{\text{in}}=125$ kW) and $S=0.2$ mm^2. The smallness of the conversion efficiency enlights the difficulty to measure $I^{2\omega}_{\text{out}}$ and the problems to eliminate the important infrared incident beam in the detection device.

For further studies about the particle origin of SHG, we give the values of the second-order polarizabilities calculated from relations (3), (6), and (15) and from the ratios between best-fit coefficients [relations (12a)]:

$$\tfrac{1}{2}|\alpha^{2\omega}_{25}-\alpha^{2\omega}_{14}|=(0.83\pm0.43)\times10^{-48}\ \text{J m}^3\ \text{V}^{-3}, \quad (16)$$

$$\tfrac{1}{2}(\alpha^{2\omega}_{31}+\alpha^{2\omega}_{32})=(1.21\pm0.44)\times10^{-48}\ \text{J m}^3\ \text{V}^{-3},$$

$$\tfrac{1}{2}(\alpha^{2\omega}_{15}+\alpha^{2\omega}_{24})=(0.57\pm0.28)\times10^{-48}e^{i(0.52\pm0.04)}\ \text{J m}^3\ \text{V}^{-3},$$

$$\alpha^{2\omega}_{33}=(1.18\pm0.59)\times10^{-48}e^{i(2.61\pm0.05)}\ \text{J m}^3\ \text{V}^{-3}.$$

V. GEOMETRICAL ASPECTS OF THE MAGNETIC PARTICLE AND ORIGIN OF THE SHG ACTIVITY

A. Particle size

Moreover, the same fitting gives a value for the ratio μ/kT. Our model takes into account the local magnetic field which results from the magnetic interactions between particles by an effective field B_{eff} which is larger than the measured one [$\mu B_{\text{eff}}/kT=\mu B/kT+\lambda\mu_0 m_S\Phi(\mu/kT)L_1(\mu B_{\text{eff}}/kT)$].[32] This correction is justified here by the important particle volume fraction Φ. λ is a dimensionless parameter ($\lambda=0.22$ from Ref. 32), m_S is the particle magnetization at saturation equal to 3.05×10^5 A/m for cobalt ferrite particles.[26] The ratio μ/kT obtained from the fitting presented in Figs. 4(a) and 4(b) is $\mu/kT=323.0\pm16.7\ \text{T}^{-1}$. The magnetic moment μ depends on m_S and on the magnetic diameter d of the particle, as follows: $\mu=m_S\pi(d^3/6)$. The temperature of the sample in the laser illuminated area lies between 300 K (room temperature) and 373 K (boiling-destruction temperature). In this temperature range, the value obtained for μ/kT leads to a diameter of 21.1 ± 1.1 nm for the grains.

In our model, the particle size is monodispersed but usually the magnetic fluids are supposed to obey a log-normal distribution.[34] The mean size of our particles, determined by x-ray measurements, is 14.1 nm whereas the values of the most probable diameter d_{mp} and of the standard deviation σ of the log-normal distribution, determined by our static birefringence measurements according to the technique given in Ref. 35, are, respectively, $d_{\text{mp}}=11$ nm and $\sigma=0.3$. The moment of the size distribution in a SHG experiment depends on the magnetic field strength (weak or at saturation) and it also depends on the origin of SHG in particles (bulk or surface process). From Eqs. (3), (6), (A6), (11) and the latter hypotheses, the size distribution moment is found to range from 0 to 12. If we take the highest value for the distribution moment, the log-normal polydispersity model gives from the above static birefringence results a 20.7 nm diameter which is in rather good accordance with the size found by the SHG experiment. However, if the distribution moment is smaller than 12, it is possible that the sample contains a more important proportion of large particles (or aggregates) than in the log-normal distribution, which would favor the SH intensity. With magnetic fluids, such a problem has already been encountered in dynamic birefringence measurements.[36]

B. Lacks of symmetry and structure of the particles

Some hypotheses can be presented about the origin of the nonlinear polarizability of the particle but before, let us resume what we know about the symmetry of this tensor. First, the properties of the single particle of our model are actually the averages of the properties of all the real ones with identical crystalline lattices. Point symmetry groups including improper rotations cannot be obtained at the end of an averaging process on a symmetryless particle because it is the result of proper rotations only. Conversely, as a ferrofluid under field cannot be centrosymmetrical because of its SHG activity and, as a C_∞ symmetry and not a $C_{\infty v}$ one, is experimentally observed, it proves, for the single particle, two different lacks of symmetry versus improper rotations, the first one being the noncentrosymmetry, the second one being also

called chirality. Some of the characteristics of the particle can be guessed from those of the intrinsic averaged polarizability tensor. It is worth noticing that, at first sight, a confusion is often made between this intrinsic averaged tensor and an ill-defined ''averaged radius particle'' which would in fact show a cylindrical $C_{\infty v}$ symmetry. In short the intrinsic averaged polarizability tensor is not centrosymmetrical and exhibits a C_{∞} symmetry. Magnetic crystal (or point) symmetry groups are not used here, they would bring no new information.

If we go into the origin of SHG more thoroughly it is better to discuss now the nature of the real particles rather than that of the model one. If individual particles were just pieces of perfect cubic crystal, their SHG activity could only arise from an asymmetry of their shape which would break the centrosymmetry of the bulk spinel ferrite structure. The particle surface is effectively known to be ''rocklike.'' Moreover two extra observations weaken this assumption. First it has been seen that the boundary zone of the particle is nonmagnetic, which is a sign that the spinel structure is modified in it;[26] is this zone amorphous or only ill-crystallized? Second the citrated particles we use are clothed by electrically charged molecules, which ensures the repulsion between particles and therefore the stability of the colloid. This complexation due to covalent bonds between each particle and surrounding citric acid molecules may introduce asymmetries.[37] These two facts may also contribute to some lost of symmetry for the whole system.

The former considerations which deal with the ability for a particle to generate second harmonic, provide no information about its magnitude. If particles are made up of three parts, a semiconductor crystalline core, a boundary zone and an outer molecular shell, the separation between surface effects given by discontinuities in the electric[28,29] or magnetic properties[11] and bulk effects cannot be achieved in such small systems. Particles must be considered as a whole and the role of quantum confinement cannot be overlooked. In these quantum confined nanostructures (quantum dots), the magnitude of the second-order polarizability depends on the potential asymmetry which can be affected by confinement.[38]

C. Origins of the asymmetries of the particle nonlinear averaged tensor

Knowing the different locations in the particle where asymmetries could appear, a question still remains without any answer: Why does the ''averaged particle'' exhibit such an asymmetry whereas it seems reasonable to think that the size and shape averaging process should destroy the asymmetries of the real particle even before the orientational averaging? The two observed lacks of symmetry will be considered separately. Let us begin with the lack of ''vertical plane'' symmetry. A symmetryless real particle gives for $\langle \alpha'^{2\omega}_{25} \rangle_{\psi}$, after a rotational averaging around $\boldsymbol{\mu}$, a nonzero value. The symmetrical particle obtained by a ''vertical'' mirror plane keeping $\boldsymbol{\mu}$, gives for $\langle \alpha'^{2\omega}_{25} \rangle_{\psi}$, the opposite value if purely electronic asymmetry effects arising from the particle magnetic moment are neglected. Therefore in this case a measured nonzero value for d_{25} proves that the particle population, giving a positive value for $\langle \alpha'^{2\omega}_{25} \rangle_{\psi}$, is not equal to the particle population giving a negative one. The chirality observed in the second-order susceptibility of the magnetic colloid under an applied magnetic field, is therefore due to the difference of the contributions of these two types of population, one of them dominating. If $\boldsymbol{\mu}$ had no other correlation with the particle atomic structure than of being bound to the particle core crystal lattice, there should be as many particles with a precise atomic structure as with the mirror one and this would give a zero $\langle \alpha'^{2\omega}_{25} \rangle_{\Omega}$ value. In this case a weak nonzero value for d_{25} could be observed in the case of an unlikely population fluctuation or if the electronic asymmetry due to the particle magnetic moment is no more negligible. Both assumptions seem unable to account for the magnitude of $\langle \alpha'^{2\omega}_{25} \rangle_{\Omega}$. The atomic structure of the clothed particle is therefore correlated with $\boldsymbol{\mu}$ which entails its chirality property. The magnetic moment $\boldsymbol{\mu}$ may bring asymmetric distortions in the core, in the boundary zone or in the covalent bonds. The origin of this correlation could also arise from the particle synthesis process; in fact however small the particle may be, it is already a magnetic monodomain and the atoms or molecules which stick to it during the synthesis period, feel the magnetic field created by the magnetic moment of the ''young'' particle.[22] Another possibility is to consider aggregates of particles whose existence has already been encountered.[36] In this case the ''particle'' studied by the statistical model would be the aggregate itself. The lack of symmetry which is discussed above could be due to the position of the particles in the structure of the aggregate.

The same reasoning can be followed for the observed lack of inversion symmetry of the magnetic fluid under an applied magnetic field. If certain values are found for $\langle \alpha'^{2\omega}_{15} \rangle_{\Omega}$, $\langle \alpha'^{2\omega}_{33} \rangle_{\Omega}$, and $\langle \alpha'^{2\omega}_{31} \rangle_{\Omega}$ after a rotational averaging on a symmetryless particle, the particle obtained from the first one by an inversion, provides opposite values for $\langle \alpha'^{2\omega}_{15} \rangle_{\Omega}$, $\langle \alpha'^{2\omega}_{33} \rangle_{\Omega}$, and $\langle \alpha'^{2\omega}_{31} \rangle_{\Omega}$. We find a similar conclusion to the one obtained for chirality: there is a correlation between the atomic structure of the real particles and their magnetic moment $\boldsymbol{\mu}$. This correlation entails also the noncentrosymmetrical properties of the averaged particle even before the rotational averaging and the noncentrosymmetrical properties of the fluid.

CONCLUSION

Second harmonic generation in magnetic colloids is made possible by applying to them a static magnetic field which breaks their fluid isotropy. We measure the macroscopic nonlinear elements of the third-rank electric susceptibility tensor of the magnetic colloid and find that its symmetry is C_{∞} and not $C_{\infty v}$.

We assume that the microscopic origin of the second-order polarization of the medium is located inside the magnetic particles and that the magnetic field orientates the particle magnetic moments, bound to their crystalline frames, in a favored direction. A link between the microscopic polarizability and the macroscopic SH susceptibility which becomes nonzero by a Boltzmann's statistical effect in presence of a magnetic field, has to be found. We propose a Langevin-like model in which all the particles are identical and independent. The identity of the particles arises from a first size and shape averaging of the real particles with identical crystalline lattices. The statistical calculation of the nonlinear susceptibility tensor components as a function of applied magnetic field strength and temperature, takes into account the three

degrees of freedom (i.e., Eulerian angles) of the particle. Among the nonzero susceptibility components, four of them are independent. One would vanish for a $C_{\infty v}$ symmetry; it is the signature of an average chirality of the particles and is ruled by the even second-order Langevin function of the Langevin parameter $\mu B/kT$. The other three independent components are the sums of a saturation value term, weighted by the first-order Langevin function, and of a coupling term weighted by a combination of first- and third-order Langevin functions. These three parameters are odd functions of the Langevin parameter. The saturation values of the susceptibility tensor elements are deduced by simple volume proportionality relations from the polarizability tensor elements; the coupling term arises from the orientational disorder of the particles at low magnetic field.

The parameter values of this model are fitted simultaneously to four independent experimental SHG intensity curves as a function of the applied field intensity. The coupling term due to the colloid orientational disorder enables us to even determine the relative phases of the complex values of some particle polarizability tensor components. It makes this determination very precise. The validity of this Langevin-like model is not only proved by the very good consistency between theoretical curves and data but also by other observed angular characteristics of the output SH beam such as its ellipticity. The statistical determination provides a value for the size of the magnetic particles which is consistent with values found by other techniques. Moreover a surface second harmonic generation phenomenon is experimentally evidenced for an oblique incidence of the laser beam. It seems that the magnetic field orientating role should be replaced by that of the surface normal but a general study, similar to the present bulk one, has to be done. In particular, the energetic aspect of the link between the magnetic particle submitted to a static magnetic field and a surface should be interesting.

Some hypotheses about the origin of SHG in our particles, the last step of our work, are expressed from considerations about the point symmetry group of the MF under static magnetic field. In our statistical orientation model, the identical particles must be noncentrosymmetrical to exhibit a bulk SH polarization: the lost of their symmetry arises from their shape but also from their atomic structure which is not that of a ferrite crystal because of size and surface complexation effects. Moreover, the magnitude of SHG may be connected to quantum confinement properties of these nanostructures. Finally, it is shown that there is a correlation between the magnetic moment and the atomic structure of the particles, the magnetic moment causing asymmetrical distorsions during the particle synthesis period. An aggregation of particles may also play the same role as the particle synthesis step for the noncentrosymmetry and for the chirality properties of the fluid.

ACKNOWLEDGMENTS

We are indebted to S. Neveu for providing us with the ferrofluid sample and for doing the corresponding x-ray measurements, to N. Piccioli for the GaP sample, to P. Lepert and J. Servais for technical assistance, to Bror M. Heegaard, V. Cabuil, A. Levelut, and Yu. Raikher for helpful discussions. We also thank P. and M. Gadenne for the use of the spectrophotometer Cary 05 for absorption measurements.

APPENDIX A: CALIBRATION FORMULAS FOR BULK SHG IN A LOSSY MEDIUM UNDER NORMAL INCIDENCE

One of the goals of this paper is to characterize the particles through their nonlinear polarizability coefficients. For that purpose, we propose the following treatment in which we use the input E_{in}^{ω} and the output $E_{\text{out}}^{2\omega}$ electric fields in vacuum which are the only observable quantities. We restrict the following presentation to experiments in which the incident beam has a normal incidence on the cell ($\psi_\omega=0°$). Appendix B is devoted to the study of the general case ($\psi_\omega\neq 0$). With the notations defined in Fig. 2, the components of the incident electric field at ω and of the output one at 2ω are in vacuum:

$$\begin{aligned} &E_{\text{in } x'}^{\omega}=0, && E_{\text{out } x'}^{2\omega}=0,\\ &E_{\text{in } y'}^{\omega}=E_{\text{in}}^{\omega}\sin\theta_\omega, \quad \text{and} && E_{\text{out } y'}^{2\omega},\\ &E_{\text{in } z'}^{\omega}=E_{\text{in}}^{\omega}\cos\theta_\omega, && E_{\text{out } z'}^{2\omega}. \end{aligned} \tag{A1}$$

We consider the SHG in a plane-parallel plate of lossy material in the case of normal incidence.[33] We use the transmission factor defined in Ref. 33, taking into account the multiple reflexions of the beams at ω and 2ω in the nonlinear medium. It is needed in the view of a calibration of the experimental SH intensities for magnetic fluids with respect to a reference sample. In our case, one needs to calculate it with the fused silica as input and output media. We neglect the plane-parallel plate effects in the glass cell so that the i components of the incident electric field in the fused silica medium $E_{G\,i}^{\omega}$ and of the output one $E_{\text{out } i}^{2\omega}$ in vacuum are written as

$$E_{G\,i}^{\omega}=E_{\text{in } i}^{\omega}\,t^{\omega},$$

$$E_{\text{out } i}^{2\omega}=E_{G\,i}^{2\omega}\,t^{2\omega}, \tag{A2}$$

where $t^{\omega}=2/(1+n_G^{\omega})$ and $t^{2\omega}=2n_G^{2\omega}/(1+n_G^{2\omega})$ are the Fresnel transmission coefficients between vacuum and the silica cell at the frequencies ω and 2ω, respectively. n_G^{ω} and $n_G^{2\omega}$ are the refractive indices of the fused silica cell containing the sample at the frequencies ω and 2ω [$n_G^{\omega}=1.4493$ at 1.064 μm and $n_G^{2\omega}=1.4604$ at 0.532 μm (Ref. 39)].

Under an applied magnetic field, the magnetic fluid becomes optically uniaxial, the extraordinary axis being parallel to the field.[31] The angle θ_ω in vacuum corresponds to an angle θ'_ω in the nonlinear medium. If the laser beam polarization is parallel to the principal axes of the ellipsoid of indices, θ'_ω is equal to 0° or 90° and it is the case for θ_ω too. Let us define the ordinary and the extraordinary complex refractive indices of the magnetic fluid at ω and 2ω by n_o^{ω}, n_e^{ω}, $n_o^{2\omega}$, and $n_e^{2\omega}$, respectively. The ordinary and the extraordinary SH wave vectors $\mathbf{k}_o^{2\omega}$ and $\mathbf{k}_e^{2\omega}$ in the medium remain both perpendicular to the cell plane: from Eqs. (8) and (A1), we see that the three components of $\mathbf{P}^{2\omega}$ are generally nonzero, $P_{x'}^{2\omega}$ and $P_{y'}^{2\omega}$ corresponding to the ordinary part of the SH polarization vector, $P_{z'}^{2\omega}$ to the extraordinary one. $P_{x'}^{2\omega}$ is a nonpropagative component. The electromag-

netic radiation at 2ω is generated by the components $P_{y'}^{2\omega}=P_o^{2\omega}$ and $P_{z'}^{2\omega}=P_e^{2\omega}$ of the SH polarization vector perpendicular to the SH wave vectors $\mathbf{k}_o^{2\omega}$ and $\mathbf{k}_e^{2\omega}$.[40] With the notations defined in Fig. 2, the C_∞ symmetry of the magnetic fluid yields the output SH electric field in vacuum:

$$E_{\text{out }o}^{2\omega}=2\frac{d_{24}}{\varepsilon_0}H_{ooe}E_{\text{in }o}^{\omega}E_{\text{in }e}^{\omega},$$

$$E_{\text{out }e}^{2\omega}=\frac{d_{32}}{\varepsilon_0}H_{eoo}(E_{\text{in }o}^{\omega})^2+\frac{d_{33}}{\varepsilon_0}H_{eee}(E_{\text{in }e}^{\omega})^2, \quad \text{(A3)}$$

where, in these normal incidence experiments, o stands for y' and e for z'. The dimensionless factor H_{ijk} is given by Eq. (A2) and a generalization of Eq. (22a) of Ref. 33. Transmission factors, birefringence, and dichroism effects for the different configurations of polarization are included in H_{ijk}. We give, for example, the expression of H_{ijk} for an incident field at ω ordinary polarized, the output beam at 2ω being either ordinary (o) or extraordinary (e) polarized $(i=o$ or $e)$:

$$H_{ioo}=-(t^{\omega})^2t^{2\omega}\frac{2[\exp(-ik_o^{\omega}d)/(n_o^{\omega}+n_G^{\omega})]^2}{[1-R_o^{\omega}\exp(-2ik_o^{\omega}d)]^2(n_i^{2\omega}+n_G^{2\omega})}\times\left\{\frac{n_i^{2\omega}(1+R_o^{\omega})+n_o^{\omega}(1-R_o^{\omega})}{(n_i^{2\omega})^2-(n_o^{\omega})^2}+\frac{2(R_o^{\omega})^{1/2}}{n_i^{2\omega}}\right\} \quad \text{(A4)}$$

with $R_o^{\omega}=[(n_o^{\omega}-n_G^{\omega})/(n_o^{\omega}+n_G^{\omega})]^2$ and $k_o^{\omega}=n_o^{\omega}(\omega/c)$. R_o^{ω} denotes the energy reflection coefficient between the glass plate and the magnetic fluid for an ordinary polarization, k_o^{ω} the ordinary wave vector at ω, and d the nonlinear material thickness. The square modulus of H_{ijk} is equal to the product of transmission factors and of F_{ijk} accounting for the Fabry-Perot effects inside the sample and defined as Φ in Ref. 33 in the simple case of a nonlinear medium surrounded by vacuum. For the ''ioo'' configuration,

$$|H_{ioo}|^2=(t^{\omega})^4(t^{2\omega})^2F_{ioo}. \quad \text{(A5)}$$

In our calculations of F_{ijk}, we assume that thickness fluctuations do not exceed the fundamental wavelength. Without applied magnetic field, the complex index values of the magnetic fluid used are $n^{\omega}=1.3641+i0.0004$ and $n^{2\omega}=1.3921+i0.0118$. The real parts of the refractive indices are measured with a dispersion corrected refractometer, and the imaginary ones with a spectrophotometer. The optical birefringence depends on the applied magnetic field strength[31] and its magnitude is about five times smaller than the very small dispersion term $n^{2\omega}-n^{\omega}$ which appears in the denominator of the H_{ijk} factor. According to our measurements at 632.8 nm, the birefringence is almost independent of temperature and is equal to 0.0061 at 0.3 T for our sample. However, its sign is undetermined. Knowing that birefringence and dichroism contributions are smaller than the dispersion one, we assume that F_{ijk} and H_{ijk} are independent of the indices i,j,k; it is useless to give an exact formulation for H_{iee} and H_{ioe}. One can calculate a mean value for F and H for any polarization configuration and any magnetic field strength. This approximation prevents us from studying the phase mismatch as a function of the magnetic field amplitude. With the above values, the coherence length is about 8.8 μm when absorption is neglected.

The temperature in the laser impact area cannot be evaluated. Sample temperature ranges between 300 and 373 K and F is calculated with the real part values of the refractive indices at 323 K and the imaginary ones at room temperature (the imaginary parts appear in F only as a small difference which does not change very much with temperature). The value of $|H|^2$ is then 8.60 for $d=10$ μm.

In the view of an analogy with Eq. (1), we define the following effective nonlinear electric susceptibility coefficients as

$$D_{im}=d_{im}H. \quad \text{(A6)}$$

D_{im} are complex quantities as it is shown by a polarization analysis (Fig. 6). It comes from the Fabry-Perot effects in the sample cell (dimensionless complex factor H) and from the fact that d_{im} coefficients can be complex. From (A3) and (A6), one obtains the following calibration expression:

$$E_{\text{out }i}^{2\omega}=\frac{D_{im}}{\varepsilon_0}(E_{\text{in}}^{\omega}E_{\text{in}}^{\omega})_m.$$

APPENDIX B: CALIBRATION FORMULAS FOR BULK SHG IN A LOSSY MEDIUM UNDER OBLIQUE INCIDENCE

This appendix is devoted to the transmitted SH intensity at the output of the cell, in the case of an oblique incidence of the laser beam on the sample. This oblique incidence is needed to determine the nonlinear term $\langle\alpha'^{2\omega}_{25}\rangle_\Omega$ and involves refractive and birefringence effects. This term includes a surface contribution $\alpha_{S\,25}'^{2\omega}$ due to the tilted cell. In the geometry used (Fig. 2), the magnetic field **B** is still parallel to the cell surface and **B** and $\mathbf{k}^{\omega}$ remain perpendicular to the rotation axis (Oy') of the cell. The treatment of birefringence and dichroism is therefore simplified because the plane of incidence contains **B** which is parallel to the revolution axis of the ellipsoid of indices. Ordinary rays are polarized perpendicularly to the plane of incidence and extraordinary rays are parallel polarized (the notations o and e are equivalent to $\perp$ and $\parallel$, respectively). But for the same reasons as in Appendix A, birefringence and dichroism effects can be neglected in front of dispersion effects.

We can then apply the formulas given by Bloembergen and Pershan[40] in the case of an oblique incidence of the laser beam on a nonlinear isotropic plane-parallel plate. They are still valid if absorption effects, important in cobalt ferrite ferrofluids, are considered. At the boundary between the linear and the nonlinear media, two light waves contribute to the SH signal: one is the free wave of wave vector $\mathbf{k}^{2\omega}$, refracted in the nonlinear medium with an angle $\psi'_{2\omega}$, and the other one is the forced wave of wave vector $2\mathbf{k}^{\omega}$, refracted with an angle ψ'_{ω}, according to the expressions used by Kleinman.[41] The laser beam incidence angle in the air is $\psi_{\omega}=40°$. It corresponds, in the magnetic fluid, to an angle of refraction $\psi'_{\omega}=28.12°$ for the fundamental and the forced SH waves and to $\psi'_{2\omega}=27.51°$ for the free SH wave (Fig. 7). As the SH wave is generated all over the sample thickness (10 μm) and as the free one follows a direction

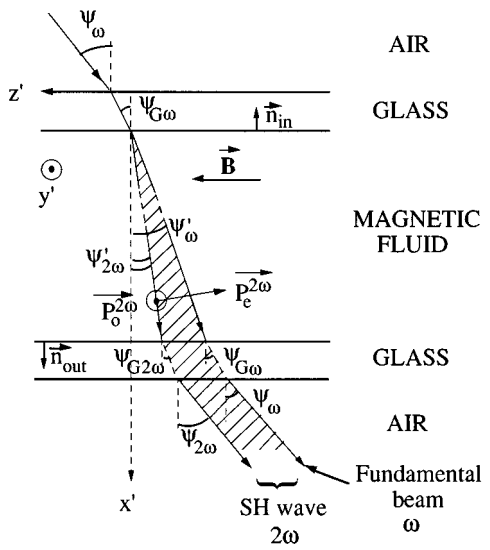

FIG. 7. Scheme of the cell: refracted rays of the fundamental and of the second harmonic beams inside the sample. Actually the MF thickness is 10 μm, much smaller than the glass one (2 mm).

different from that of the fundamental one, the SH beam is broadened of about 0.1 μm at the output of the magnetic fluid and finally of 9.5 μm at the output of the cell. It is completely negligible compared to the width of the infrared incident beam which is, in the experiment, focused outside of the cell to avoid sample destruction.

The experiment at $\psi_\omega \neq 0$ is done for $\theta_\omega = 0°$ and $\theta_{2\omega} = 90°$ [curve (D) in Fig. 4(b)], which corresponds to the following components of the incident electric field at ω and of the output one at 2ω in vacuum:

$$\begin{aligned} &E^{\omega}_{\text{in } x'} = -E^{\omega}_{\text{in}} \sin\psi_\omega, && E^{2\omega}_{\text{out } x'} = 0, \\ &E^{\omega}_{\text{in } y'} = 0, \quad \text{and} && E^{2\omega}_{\text{out } y'} = E^{2\omega}_{\text{out}}, \\ &E^{\omega}_{\text{in } z'} = E^{\omega}_{\text{in}} \cos\psi_\omega, && E^{2\omega}_{\text{out } z'} = 0. \end{aligned} \tag{B1}$$

As in Appendix A, the factor H_{oblique} is determined by neglecting the multiple interferences effects in the fused silica walls which are the input and output media of the active medium; for an oblique incidence of the laser beam on the cell and for $\theta_\omega = 0°$, the ordinary and extraordinary components of the incident electric field are given by $E^{\omega}_{G\,o} = E^{\omega}_{G\,x'}$ and $E^{\omega}_{G\,e} = E^{\omega}_{G\,z'}$, and for $\theta_{2\omega} = 90°$, the output electric field has only an ordinary polarization:

$$E^{\omega}_{G\,o} = E^{\omega}_{\text{in } o}\, t^{\omega}_o,$$

$$E^{\omega}_{G\,e} = E^{\omega}_{\text{in } e}\, t^{\omega}_e,$$

$$E^{2\omega}_{\text{out } o} = E^{2\omega}_{G\,o}\, t^{2\omega}_o,$$

where t^{ω}_o, t^{ω}_e, and $t^{2\omega}_o$ are the different Fresnel transmission coefficients according to the frequency and the polarization direction of the laser beam:

$$t^{\omega}_o = \frac{2\cos\psi_\omega}{\cos\psi_\omega + n^{\omega}_G \cos\psi_{G_\omega}},$$

$$t^{\omega}_e = \frac{2\cos\psi_\omega}{n^{\omega}_G \cos\psi_\omega + \cos\psi_{G_\omega}},$$

$$t^{2\omega}_o = \frac{2 n^{2\omega}_G \cos\psi_{G_{2\omega}}}{n^{2\omega}_G \cos\psi_{G_{2\omega}} + \cos\psi_\omega}. \tag{B2}$$

The refractive indices, n^{ω}_G and $n^{2\omega}_G$, and the corresponding angles of refraction, ψ_{G_ω} and $\psi_{G_{2\omega}}$, refer to the fundamental and SH waves in the fused silica cell, respectively (see Fig. 7). The SH radiation is generated by the three components of the second-order polarization vector whose ordinary and extraordinary parts are

$$P^{2\omega}_e \mathbf{e}_e = P^{2\omega}_{z'} \mathbf{e}_{z'},$$

$$P^{2\omega}_o \mathbf{e}_o = P^{2\omega}_{x'} \mathbf{e}_{x'} + P^{2\omega}_{y'} \mathbf{e}_{y'},$$

where $\mathbf{e}$ are the different unit vectors. $P^{2\omega}_e$ and $P^{2\omega}_o$ are equivalent to $P^{\text{NLS}}_{\parallel}$ and $P^{\text{NLS}}_{\perp}$, respectively, in Bloembergen and Pershan's notations.[40] The analyzer keeps only the SH field generated by $P^{2\omega}_{y'}$. The SH intensity at the output of the cell (in vacuum) is given by the ordinary component of the SH electric field and from Eqs. (3), (8), and (B1):

$$I^{2\omega}_{\text{out } o} = \frac{2(I^{\omega}_{\text{in}})^2}{S\varepsilon_0 c}\, 4\cos^2\psi_\omega \sin^2\psi_\omega |H_{\text{oblique}}|^2 \left(\frac{d_{25}}{\varepsilon_0}\right)^2 \tag{B3}$$

with $S = S_0 \cos\psi_\omega / \cos\psi_{2\omega}$, S_0 being the beam section. The factor H_{oblique} is defined as

$$|H_{\text{oblique}}|^2 = (t^{2\omega}_o t^{\omega}_o t^{\omega}_e)^2 F_{\text{oblique}} \tag{B4}$$

and F_{oblique} is obtained from (6.8) and (6.9) of Ref. 40 by using the same approximation as in Appendix A, in which magnetic field induced birefringence and dichroism are neglected:

$$F_{\text{oblique}} = \left| \frac{N}{[(n^{2\omega})^2 - (n^{\omega})^2] D} \right|^2 \tag{B5}$$

whose numerator is

$$\begin{aligned} N = &- C_{2\omega}(C_{G_{2\omega}} + C_\omega)(\cos\Phi_{2\omega} - \cos\Phi_\omega) \\ &+ i[[C_{G_{2\omega}} C_\omega + (C_{2\omega})^2]\sin\Phi_{2\omega} \\ &- C_{2\omega}(C_{G_{2\omega}} + C_\omega)\sin\Phi_\omega] \end{aligned}$$

and whose denominator is

$$D = 2 C_{G_{2\omega}} C_{2\omega} \cos\Phi_{2\omega} - i[(C_{G_{2\omega}})^2 + (C_{2\omega})^2]\sin\Phi_{2\omega}$$

with $\Phi_\omega = C_\omega \omega d/c$, $\Phi_{2\omega} = C_{2\omega} \omega d/c$. The C quantities used above are complex functions of the complex refractive indices and of the complex angles of refraction ψ'_ω and $\psi'_{2\omega}$ in the magnetic fluid, defined by

$$C_{G_{2\omega}} = \sqrt{(n_G^{2\omega})^2 - (\sin\psi_\omega)^2} = n_G^{2\omega} \cos\psi_{G_{2\omega}},$$

$$C_\omega = \sqrt{(n^\omega)^2 - (\sin\psi_\omega)^2} = n^\omega \cos\psi'_\omega,$$

$$C_{2\omega} = \sqrt{(n^{2\omega})^2 - (\sin\psi_{2\omega})^2} = n^{2\omega} \cos\psi'_{2\omega}.$$

This calculation yields the following value for a calibration under oblique incidence: $|H_{\text{oblique}}|^2/|H|^2 = 0.72$.

*Also at Université de Paris VII, UFR de Physique, 2 Place Jussieu, 75251 Paris Cedex 05, France.
†Associated with the Centre National de la Recherche Scientifique.

[1] V. M. Akulin, E. Borsella, and A. A. Nesterenko, Phys. Rev. Lett. **73**, 1231 (1994).
[2] B. Jérôme and Y. R. Shen, Phys. Rev. E **48**, 4556 (1993).
[3] K. Shirota, K. Ishikawa, H. Takezoe, A. Fukuda, and T. Shiibashi, Jpn. J. Appl. Phys. **34**, L 316 (1995).
[4] R. W. Terhune, P. D. Maker, and C. M. Savage, Phys. Rev. Lett. **8**, 404 (1962).
[5] G. Mayer, C. R. Acad. Sci. (Paris) **267B**, 54 (1968).
[6] P. Voigt, K. Betzler, N. Schmidt, and S. Kapphan, Ferroelectrics **106**, 149 (1990); also, P. Voigt and S. Kapphan, *ibid*. **157**, 239 (1994).
[7] D. Gonin, Ph.D. thesis of University Paris 6, 1994.
[8] S. Sprunt, J. Naciri, B. R. Ratna, and R. Shashidhar, Appl. Phys. Lett. **66**, 1443 (1995).
[9] S. Kielich, IEEE J. Quantum Electron. **QE-5**, 562 (1969).
[10] M. Barmentlo, R. W. J. Hollering, H. A. Wierenga, C. W. van Hasselt, and Th. Rasing, Physica B **204**, 38 (1995).
[11] Th. Rasing and H. A. Wierenga, *Proceedings of the Second International Conference on Magnetoelectric Interaction Phenomena* [Ferroelectrics **162**, 217 (1994)].
[12] M. Fiebig, D. Fröhlich, B. B. Krichevtsov, and R. V. Pisarev, Phys. Rev. Lett. **73**, 2127 (1994).
[13] J.-C. Bacri, R. Perzynski, and D. Salin, Endeavour **12**, 76 (1988).
[14] J.-C. Bacri, R. Perzynski, M. I. Shliomis, and G. I. Burde, Phys. Rev. Lett. **75**, 2128 (1995).
[15] J.-C. Bacri, A. Cebers, A. Bourdon, G. Demouchy, B. M. Heegaard, and R. Perzynski, Phys. Rev. Lett. **74**, 5032 (1995).
[16] R. Massart, IEEE Trans. Magn. **17**, 1247 (1981).
[17] Yu. L. Raikher and M. I. Shliomis, Adv. Chem. Phys. **87**, 595 (1994).
[18] J.-C. Bacri and D. Gorse, J. Phys. (Paris) **44**, 985 (1983).
[19] V. Dmitriev and L. Tarassov, Optique Non Lineaire Appliqúee (Mir, Moscow, 1987), p. 304.
[20] A. Yariv, *Quantum Electronics*, 2nd ed. (Wiley, New York, 1975), p. 408.
[21] J. F. Nye, *Physical Properties of Crystals* (Clarendon Press, Oxford, 1957).
[22] P. I. Slick, in *Ferromagnetic Materials*, edited by E. P. Wohlfarth (North-Holland Physics Publishing, Amsterdam, 1986), Vol. 2, Chap. 3.
[23] A. Herpin, *Théorie du Magnétisme* (PUF and INSTN, Paris, 1968), Chap. XIX(A), p. 645.
[24] V. Cabuil and R. Perzynski, in *Magnetic Fluids and Applications Handbook*, edited by B. Berkovsky and M. Kharkov (Begell House, New York, 1994), p. 12.
[25] J. Tejada, Ll. Barcells, S. Linderoth, R. Perzynski, B. Rigau, B. Barbara, and J.-C. Bacri, J. Appl. Phys. **73**, 6952 (1993).
[26] F. Tourinho, R. Franck, R. Massart, and R. Perzynski, Prog. Colloid Polym. Sci. **79**, 128 (1989).
[27] Y. Kanemitsu, T. Ogawa, K. Shiraishi, and K. Takeda, Phys. Rev. B **48**, 4883 (1993).
[28] Y. R. Shen, *The Principles of Non Linear Optics* (Wiley & Sons, New York, 1984), Chap. 25.
[29] Y. R. Shen, in *Fundamental Systems in Quantum Optics*, edited by J. Dalibard, J. M. Raimond, and J. Zinn-Justin (Elsevier Science Publishers, British Vancouver, 1992), p. 1051.
[30] D. A. Kleinman, Phys. Rev. **126**, 1977 (1962).
[31] S. Neveu-Prin, F. A. Tourinho, J.-C. Bacri, and R. Perzynski, Colloids Surf. A **80**, 1 (1993).
[32] J.-C. Bacri, A. Cebers, A. Bourdon, G. Demouchy, B. M. Heegaard, B. Kachevsky, and R. Perzynski, Phys. Rev. E **52**, 3936 (1995).
[33] E. Bringuier, A. Bourdon, N. Piccioli, and A. Chevy, Phys. Rev. B **49**, 16 971 (1994).
[34] J.-C. Bacri, V. Cabuil, R. Massart, R. Perzynski, and D. Salin, J. Magn. Magn. Mater. **65**, 285 (1987).
[35] J.-C. Bacri and R. Perzynski, in *Magnetic Fluids and Applications Handbook* (Ref. 24), p. 76.
[36] J.-C. Bacri, R. Perzynski, D. Salin, and J. Servais, J. Phys. (Paris) **48**, 1385 (1987).
[37] J.-C. Bacri, R. Perzynski, and D. Salin, J. Magn. Magn. Mater. **85**, 27 (1990).
[38] C. Flytzanis and J. Hutter, in *Contemporary Nonlinear Optics*, edited by G. P. Agrawal and R. W. Boyd (Academic Press, New York, 1992), Chap. 8.
[39] *American Institute of Physics Handbook*, 2nd ed. (MacGraw-Hill New York, 1963), pp. 6–25.
[40] N. Bloembergen and P. S. Pershan, Phys. Rev. **128**, 606 (1962).
[41] D. A. Kleinman, Phys. Rev. **128**, 1761 (1962).